Time- and Unit-Cell Splitting Comparison for the Autonomous Operation of Reconfigurable Intelligent Surfaces

Konstantinos Ntontin⊙, *Member, IEEE*, Emil Björnson⊙, *Fellow, IEEE*,
Alexandros-Apostolos A. Boulogeorgos⊙, *Senior Member, IEEE*, Zaid Abdullah⊙, *Member, IEEE*,
Agapi Mesodiakaki⊙, *Member, IEEE*, Sergi Abadal⊙, *Member, IEEE*,
and Symeon Chatzinotas⊙, *Fellow, IEEE*

Abstract—In this work, we analytically compare the performance of the time- and unit cell-splitting protocols for satisfying the energy needs of reconfigurable intelligent surfaces (RISs) through wireless energy harvesting from information signals. We first compute the RIS energy consumption per frame for both protocols and subsequently formulate an optimization problem that maximizes the average rate under the constraint of meeting the RIS long-term energy consumption demands. Analytical solutions to the optimal allocation of resources that involve a single integral are provided for both protocols in the case of random transmitter-RIS links that are subject to Rician or Nakagami-m fading distributions. Moreover, closed-form solutions are provided for the case of deterministic transmitter-RIS links. In addition, increasing and decreasing monotonic trends are revealed, based on analysis, for the ratio of the achievable rates of the presented protocols with respect to the RIS energy consumption. Finally, numerical results validate the analytical findings and reveal that the unit cell-splitting protocol exhibits a notably higher average rate performance compared with its time-splitting counterpart throughout the feasible range of RIS energy consumption values. However, this comes at a cost of a notably reduced signal-to-noise ratio as the RIS energy demands increase.

Index Terms—Autonomous operation, reconfigurable intelligent surfaces (RISs), 6G networks, wireless energy harvesting.

NOMENCLATURE

DC	Direct Current
EH	Energy Harvesting
LoS	Line-of-Sight
MEMS	Micro-Electromechanical System
mmWave	Millimeter Wave
PIN	Positive-Intrinsic-Negative
RF	Radio-Frequency
RIS	Reconfigurable Intelligent Surface
RX	Receiver
SNR	Signal-to-Noise Ratio
STAR	Simultaneous Transmission and Reflection
TX	Transmitter
UC	Unit Cell

I. INTRODUCTION

THE MILLIMETER wave (mmWave) bands envisioned for the forthcoming 6G networks have very limited coverage and are highly susceptible to blockages. The coverage can be improved using relays but these require substantial energy consumption for signal amplification and, thus, need a dedicated power supply. An alternative paradigm is reconfigurable intelligent surfaces (RISs) that can be optimized to reflect signals around obstacles [1], [2]. Their potential has also led to the creation of a relevant industry specification group at the European Telecommunications Standards Institute [3]. Since RISs are not amplifying signals and the energy consumption is only related to the control protocols, they are often characterized as nearly passive structures. This raises the question of whether RISs can operate autonomously by being powered through wireless energy harvesting (EH). Such a disruptive feature has particularly been proposed for the so-called integrated architecture for altering the impedance of the unit cells (UCs) that relies on a network of integrated and interconnected electronic chips [4], [5], [6].

Why autonomous RISs?: Let us first identify indicative scenarios in which autonomous RIS operation is a desirable feature. Such scenarios are depicted in Fig. 1. They concern power-grid unavailability in certain outdoor locations, high maintenance costs for cable connections in ubiquitous
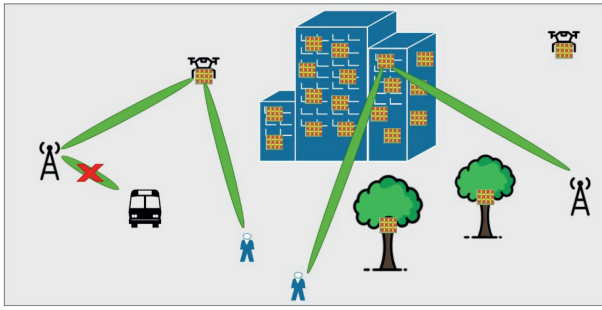
Fig. 1. Indicative scenarios in which autonomous RIS operation is desirable.

indoor deployments, and aesthetic issues that could render difficult to obtain permissions from building managers for exterior facade deployment or for deployment onto trees, for instance. Supplying their energy needs through single-use batteries that are not recharged perpetually is not a viable option, since they would need constant monitoring and manual replacement. Moreover, all competing coverage-extending technologies (e.g., relays and small cells) require power-grid availability, so a gridless RIS operation would fill an empty gap.

Related works: A few recent works have started incorporating the feature of RIS autonomy by wireless EH from information signals or dedicated power beacons, leveraging either time splitting [7], [8], or UC/power splitting [9], [10], [11], [12], or both protocol types [13]. In the time-splitting case, dedicated disjoint time intervals are allocated for either EH through absorption or information transmission through reflection. In the UC/power-splitting one, there is a common time interval for both EH and information transmission where either a subset of UCs is dedicated to EH and its orthogonal complement subset to information transmission or the reflection coefficient of all the UCs is properly adjusted so that a part of the impinging on the RIS power is absorbed to supply its energy needs and the rest is reflected towards the intended destination for information transmission. In detail, regarding the aforementioned works, in [7] the authors investigate the throughput maximization problem of an RIS-assisted multiple-input and single-output system with a power budget constraint for the RIS. They proposed a time-based protocol for the RIS to harvest energy in the first phase and, subsequently, assist the information transmission in the second phase. Again, under the consideration of a time-based protocol, in [8] the authors leverage an RIS to assist energy transmission in the first phase to a group of sensor nodes from a dedicated energy source that dispatches power beacons while the sensors transmit information in the second phase to an access point. The first phase is divided into two periods. In the first period, the RIS harvests energy to supply its operations while in the second one it uses the harvested energy to reflect the impinging power to the sensors for energy transmission.

Moving away from time-based protocols, in [9] the authors study the joint design of beamformers at an access point and the phase shifts as well as the energy harvesting schedule at an RIS for maximizing the system sum-rate. The RIS dedicates a portion of the UCs to EH and the rest to information transmission. Instead of dedicating disjoint UC subsets to EH and information transmission, the authors in [10] adjust the

reflection coefficient of the UCs so that a portion is absorbed for supplying the RIS energy needs and the rest is reflected for both information and power transmission to information and energy users, respectively. As a design aim, the authors target the maximization of the information users' sum data rate while guaranteeing the power harvesting requirements of the energy users and the RIS. In [11] the authors study the joint problem of optimal RIS placement and its proper phase and amplitude response adjustment so that the instantaneous signal-to-noise ratio (SNR) at the intended destination is maximized while at the same time the energy consumption demands of the RIS are met through EH from the impinging information signals. On the other hand, for the case of random channel links and disjoint subsets used for RIS EH and information transmission, low-complexity algorithms that are based on channel-gain ordering are considered in [12]. The aim is to properly allocate the subsets so that the instantaneous SNR is maximized while again the RIS energy consumption demands are met. Finally, to the best of our knowledge, only [13] considers both time- and UC-splitting protocols for RIS EH so that its operations are sustained. The target is the simultaneous improvement of the performance of downlink energy transfer from a hybrid access point to multiple users and uplink information transmission from users to the access point. The authors show by simulations that the UC-splitting scheme can outperform its time-splitting counterpart when the transmit power at the access point is high enough or the channel between the access point and the RIS is of good quality.

Motivation and contribution: The state-of-the-art works on resource allocation for autonomous RISs [7], [8], [9], [10], [11], [12], [13] consider online resource allocation approaches based on instantaneous channel estimates, which increase the allocation complexity. Apart from this, in previous works there has been no comparison conducted through mathematical analysis of the time-splitting and UC-splitting protocols, which are the ones that have been considered most in the literature. To the best of our knowledge, such a comparison has been provided in [12] and [13], but only through simulations. Furthermore, previous works largely overlook the RIS energy consumption related to the reconfigurations needed for channel estimation. However, this incorporation is essential since, as [12] revealed which is the only literature work to the best of our knowledge that has incorporated this, the RIS energy consumption resulting from channel estimation could be at least equal to the one associated with the reconfigurations needed for information transmission.

Based on the above, the contribution of this work can be summarized as follows:

- We present time-splitting and UC-splitting wireless EH protocols for RISs that incorporate the channel estimation phase. This allows us to accurately compute the RIS energy consumption during a transmission frame. In addition, for the considered channel estimation scheme, we prove that the energy consumption part of the RIS that is related to channel estimation is much larger than the one that corresponds to the need for UC impedance reconfiguration for EH and information transmission.

- In contrast to previous works that consider online resource allocation based on instantaneous channel estimates, we consider low-complexity offline resource allocation problems for the two presented protocols, based on the long-term statistics of the rate. Analytical solutions that target the average rate maximization, which involve a single integral, are provided for the case of random transmitter (TX)-RIS links that are subject to the widely used, based on experimental studies, Rician and Nakagami-m distributions, which incorporate a strong line-of-sight (LoS) component. In addition, closed-form solutions are provided in the case of deterministic TX-RIS channel gains. Finally, we prove that the ratio of the achievable rate in the UC-splitting protocol case over the corresponding rate of its time-splitting counterpart exhibits monotonic trends with respect to the RIS energy consumption that are different in the high- and low -SNR regions of the former protocol.

The rest of this manuscript, which is an extension of our work in [14],[1] is structured as follows. In Section II, the system and channel models are presented together with the considered channel estimation protocol and the employed power consumption model. In Section III, we initially compute the harvested energy per transmission frame. Subsequently, we introduce the proposed time- and UC-splitting protocols and compute the RIS energy consumption per frame for both protocols. Additionally, we prove that the energy consumption related to channel estimation is much higher than the one needed for both EH and information transmission. Finally, we compute the instantaneous SNR and achievable rate for both protocols. In Section IV, the formulation of the problem of interest is presented together with an analytical solution that involves a single integral and a term that depends on the TX-RIS channel distribution in the case of random TX-RIS links. Moreover, closed-form solutions are provided for the two considered protocols in the case of deterministic TX-RIS channel gains. In Section V, we compute closed-form formulas for the mentioned term of the analytical solution in the case of the TX-RIS links following the Rician and Nakagami-m distributions. Furthermore, we prove monotonic trends of the ratio of the achievable average rate of the UC-splitting protocol over its time-splitting counterpart with respect to the RIS energy consumption. Numerical results that substantiate the analytical findings are presented in Section VI, while the main takeaways of this work are summarized in Section VII.

II. SYSTEM, CHANNEL, AND RIS POWER-CONSUMPTION MODEL

In this section, we first present the system model under consideration. Subsequently, we introduce the channel model and the assumed channel-estimation protocol. Finally, we present the considered RIS power-consumption model.
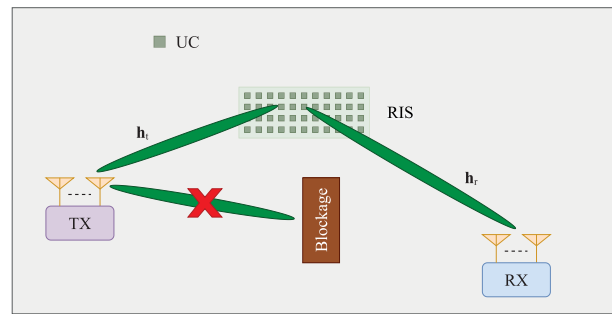

Fig. 2.   RIS-assisted communication due to a blocked direct link.

A. System Model

As illustrated in Fig. 2, we consider a scenario in which a directional TX communicates with a directional receiver (RX) through an RIS located in the far-field of both the TX and RX. The TX and RX antennas are planar arrays equipped with a number of antennas in the x- and y-axis equal to M_{T_x} (M_{r_x}) and M_{T_y} (M_{r_y}), and adjacent element distance equal to d_{T_x} (d_{R_x}) and d_{T_y} (d_{R_y}), respectively. Hence, for their total number of antennas, defined by M_T and M_R, respectively, it holds that $M_T = M_{T_x} \times M_{T_y}$ and $M_R = M_{R_x} \times M_{R_y}$. In addition, the TX-RIS link, of distance d_t m, and RIS-RX link, of distance d_r m, constitute an alternative path to the direct TX-RX link that is assumed to be blocked. The RIS is a rectangular uniform planar array consisting of $M_s = M_{s_x} \times M_{s_y}$ UCs of size $d_{s_x} \times d_{s_y}$. M_{s_x} (M_{s_y}) and d_{s_x} (d_{s_y}) denote the number of UCs and their length in the *x*-axis (*y*-axis), respectively. We assume that the RIS is not equipped with an external power supply, but it relies on EH from the signals transmitted by the TX. Through this harvested energy, it can achieve autonomous operation. The transmission power of TX is denoted by P_t.

B. Channel Model

We assume a flat-fading[2] channel model with a dominant LoS component for both the TX-RIS and RIS-RX links.[3] By $\mathbf{w}_t \in \mathbb{C}^{1 \times M_t T}$, $\mathbf{w}_r \in \mathbb{C}^{1 \times M_R}$, $\mathbf{H}_t \in \mathbb{C}^{M_s \times M_T}$, and $\mathbf{H}_r \in \mathbb{C}^{M_R \times M_s}$ we denote the transmit beamforming vector, the receive beamforming vector, the TX-RIS channel, and the RIS-RX channel, respectively. Then, the received signal, denoted by y_r, is given by:

$$
\begin{aligned}
y_r &= \mathbf{w}_r \mathbf{H}_r \begin{pmatrix} e^{j\varphi_1} & \cdots & 0 \\ 0 & \ddots & 0 \\ 0 & 0 & e^{j\varphi_{M_s}} \end{pmatrix} \mathbf{H}_t \mathbf{w}_t^T \\
&= \mathbf{h}_r \begin{pmatrix} e^{j\varphi_1} & \cdots & 0 \\ 0 & \ddots & 0 \\ 0 & 0 & e^{j\varphi_{M_s}} \end{pmatrix} \mathbf{h}_t^T,
\end{aligned}
\tag{1}
$$

---

where

$$\mathbf{h}_t = \mathbf{w}_t \mathbf{H}_t^T = \begin{bmatrix} h_{t_1} & h_{t_2} & \cdots & h_{t_{M_s}} \end{bmatrix},$$
$$\mathbf{h}_r = \mathbf{w}_r \mathbf{H}_r = \begin{bmatrix} h_{r_1} & h_{r_2} & \cdots & h_{r_{M_s}} \end{bmatrix} \qquad (2)$$

and $\phi_1, \ldots, \phi_{M_s}$ are the phase shifts of the UCs of the RIS.

The complex envelope channel vectors $\mathbf{h}_t$ and $\mathbf{h}_r$ describe the joint effect of antenna gains, geometric pathloss, and multipath fading (i.e., the combination of small-scale and large-scale fading). Based on these assumptions, they are time-varying due to multipath fading, which calls for a time-varying RIS configuration. Furthermore, we consider a block-fading model where the channel vectors are fixed within fixed-size time intervals, but change abruptly between intervals. Due to the existence of a dominant LoS component and in order to alleviate the burden of channel estimation of all the TX-RIS-RX channel when the TX and RX are equipped with a very large number of antennas, we further assume that the TX and RX antennas are phase aligned with the RIS direction. Hence, $\mathbf{w}_t$ and $\mathbf{w}_r$ are solely determined by the angle of departure and angle of arrival, respectively, of the LoS component [17].[4] Consequently, the channel estimation of the cascaded TX-RIS-RX channel concerns only the estimation of the M_s $\mathbf{h}_t \odot \mathbf{h}_r$ links related to each RIS UC instead of estimating $M_T \times M_s \times M_R$ links that would be required if $\mathbf{w}_t$ and $\mathbf{w}_r$ are optimized based on the individual TX-RIS-RX links.

C. Channel-Estimation Protocol

For the estimation of the individual $\mathbf{h}_t$ and $\mathbf{h}_r$ links form the cascaded $\mathbf{h}_t \odot \mathbf{h}_r$ ones, we consider the approach presented in [18]. According to [18], for effective recovery of $\mathbf{h}_t$ and $\mathbf{h}_r$ during each time slot of the preamble duration of a frame,[5] which we denote by N_{pr}, some of the UCs are in the 'Off' state (0 value) and some in the 'On' state (1 value) and the position of 0's and 1's changes at each slot. The UC states "Off" and "On" denote the cases where there is only a structure-mode reflection ("Off" state) or both structure and antenna-mode reflection ("On" state) [18]. We further denote the percentage of UCs that are in state '1' at each slot of the preamble by μ. As stated in [18], the recovery of the TX-RIS and RIS-RX links is more effective for low values of μ. Based on this, in the worst-case scenario the number of state changes during the training period is equal to twice the number of its 'On' states, i.e., $2\mu N_{\mathrm{pr}}$. Hence, the upper bound $N_{\mathrm{rec}}^{\mathrm{CE}}$ on the RIS reconfigurations for channel estimation, is given by

$$N_{\mathrm{rec}}^{\mathrm{CE}} = 2 M_s \mu N_{\mathrm{pr}}. \qquad (3)$$

Moreover, regarding how channel estimation can be practically performed, the TX-RIS and RIS-RX links can be estimated at: i) either the RX in a frequency-division duplexing architecture and dispatched to the TX which is responsible to transmit wireless signals towards the RIS for reconfiguration

or ii) the TX in time-division duplexing provided that channel reciprocity holds in the TX-RIS-RX links.[6]

Remark 1: According to the previous paragraph, we implicitly make the assumption that the tuning time of each UC is much shorter than the coherence time of the channel, which dictates the duration of each frame. This can also be the case in mmWave scenarios, apart from sub-6 GHz ones, in cases that do not involve very high mobility of the users. For instance, for a typical scenario of the radiation pattern of an RIS following a pedestrian user, the Doppler shift at 28 GHz is around 100 Hz for an average pedestrian velocity of 1 m/s. Hence, by taking the inverse of this shift the channel coherence time is around 10 ms. This figure well exceeds the tuning time of common RIS actuators, such as varactors, radio frequency (RF)-switches, PIN diodes, and RF-MEMS that is in the order of either ns or μs [20]. This also means that higher velocities of the users can be accommodated and still remain within the coherence time of the channel for tuning times that can be as high as several μs.

D. RIS Power-Consumption Model

Under the consideration of the integrated control architecture, we assume that one chip controls the impedance of a single UC. Furthermore, for the RF-to-direct current (DC) power conversion that is needed to power the electronic modules of the RIS, we assume that a passive rectifier circuit follows an RF combiner that combines the absorbed RF powers related to each UC [21]. Hence, the power consumption of the RIS is only the result of the static and dynamic power consumption of the M_s electronic chips that adjust the UC impedance.

III. HARVESTED ENERGY PER FRAME, TIME/UC-SPLITTING ARCHITECTURES, RIS ENERGY CONSUMPTION, AND PERFORMANCE INDICATORS

The aim of this section is to first compute the harvested energy per transmission frame, subsequently to present the time- and UC-splitting architectures together with the resulting energy consumption per frame and, finally, to provide a complexity comparison and compute the end-to-end instantaneous SNR and achievable rate.

A. Harvested Energy Per Frame

Let us denote the set of the UCs used for harvesting (the same for each frame) by $\mathcal{A}_h$ and of all the UCs by $\mathcal{A}_s$, i.e.,

$$\mathcal{A}_s = \{1, 2, \ldots, M_s\}. \qquad (4)$$

Consequently, it holds that $\mathcal{A}_h \subseteq \mathcal{A}_s$. In addition, we denote the set of the UCs dedicated for reflection by $\mathcal{A}_r$. As a result, $\mathcal{A}_r$ is the orthogonal complement of $\mathcal{A}_h$, i.e., $\mathcal{A}_r = \mathcal{A}_h^C$. Finally, the number of UCs in $\mathcal{A}_h$ and $\mathcal{A}_r$ is denoted by M_h and M_r, respectively. Hence, $M_h + M_r = M_s$.

As for the DC harvested power at a time slot of the n_{th} frame dedicated for EH, either solely or in parallel with

---

[4]Such a simplified solution for defining $\mathbf{w}_t$ and $\mathbf{w}_r$ offers performance close to one achieved by optimizing $\mathbf{w}_t$ and $\mathbf{w}_r$ under dominant LoS channels and a large number of TX and RX antennas, according to [17].

[5]The preamble at the beginning of each frame is used for both time/frequency synchronization and channel estimation.

[6]This can be the case in several scenarios [19].
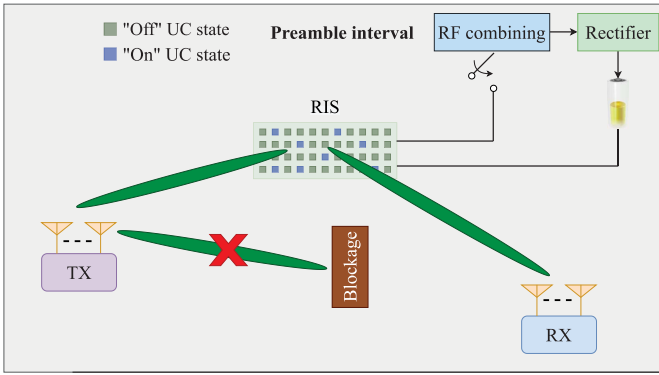
Fig. 3. Preamble phase, common for both the proposed time-splitting and UC-splitting protocols.

Fig. 4. Frame structure in the time-splitting protocol.

Fig. 5. Post-preamble time-splitting protocol functionality.

information transmission, denoted by $P_{\mathrm{DC}}(\mathcal{A}_h)$, it holds [22]

$$P_{\mathrm{DC}}(\mathcal{A}_h) = \frac{\frac{P_{\max}}{1+e^{-a(P_{\mathrm{RF}}(\mathcal{A}_h)-b)}} - \frac{P_{\max}}{1+e^{ab}}}{1 - \frac{1}{1+e^{ab}}}, \qquad (5)$$

where $P_{\mathrm{RF}}(\mathcal{A}_h)$ is the harvested RF power that is inputted to the rectifier and $P_{\max}$ is a constant denoting the maximum harvested power when the harvesting circuit at the rectifier is saturated. In addition, a and b are circuit-specific parameters, which are related to the resistance, capacitance, and turn-on voltage of the diode used for rectification. The nonlinear model of (5) has been extensively validated through experimental measurements [22].

Regarding $P_{\mathrm{RF}}(\mathcal{A}_h)$, it is given by

$$P_{\mathrm{RF}}(\mathcal{A}_h) = P_t \sum_{i \in \mathcal{A}_h} |h_{t_i}|^2, \qquad (6)$$

where P_t is the TX power. Finally, by denoting the number of time slots (the same for each frame) dedicated to EH by N_h, the time slot duration by T_{sl}, and the harvested energy by E_h, it holds

$$E_h = P_{\mathrm{DC}}(\mathcal{A}_h) N_h T_{\mathrm{sl}}. \qquad (7)$$

B. Proposed Architectures and RIS Energy Consumption

1) Proposed Time-Splitting Protocol: In the proposed time-splitting protocol, after the preamble phase that is depicted in Fig. 3 a time interval for wireless power transfer follows where all the UCs of the RIS are dedicated to EH. This interval has a duration of N_{pt} slots. Finally, the payload transmission interval follows with a duration of N_{pl} time slots where all the UCs of the RIS are dedicated to focusing towards the RX through perfect reflection. By denoting the number of time slots in a frame as N_{fr}, it holds

$$N_{\mathrm{fr}} = N_{\mathrm{pr}} + N_{\mathrm{pt}} + N_{\mathrm{pl}}. \qquad (8)$$

Illustratively, the frame structure is depicted in Fig. 4 and the functionality of the RIS for the post-preamble frame intervals is depicted in Fig. 5.

Regarding the surface reconfigurations needed per frame, apart from the $N_{\mathrm{rec}}^{\mathrm{CE}}$ reconfigurations needed for channel estimation, according to Fig. 4, M_s additional reconfigurations are needed for adjusting the UC impedances, based on the channel estimates, so to maximize the power harvested during the wireless power transfer interval. Finally, M_s additional reconfigurations are needed for adjusting the UC impedances after the wireless power transfer interval so that the RIS behaves as a reflector towards the RX. We denote the corresponding number of reconfigurations for UC impedance adjustment for wireless power transfer and for information transmission by $N_{\mathrm{rec}}^{\mathrm{PT}}$ and $N_{\mathrm{rec}}^{\mathrm{IT}}$, respectively. Consequently, it holds

$$N_{\mathrm{rec}}^{\mathrm{PT}} = N_{\mathrm{rec}}^{\mathrm{IT}} = M_s. \qquad (9)$$

As a result, for the upper bound on the total number per frame of the intelligent surface reconfigurations needed in the time-splitting protocol for channel estimation, wireless power transfer, and information transmission, which we denote by $N_{\mathrm{rec}}^{\mathrm{TS}}$, it holds

$$N_{\mathrm{rec}}^{\mathrm{TS}} = N_{\mathrm{rec}}^{\mathrm{CE}} + N_{\mathrm{rec}}^{\mathrm{PT}} + N_{\mathrm{rec}}^{\mathrm{IT}} = M_s\big(2\mu N_{\mathrm{pr}} + 2\big). \quad (10)$$

Let us now evaluate the total RIS energy consumption per frame in the time-splitting protocol, denoted by $E_{\mathrm{tot}}^{\mathrm{TS}}$. It holds that [23, Eq. (4.5)]

$$E_{\mathrm{tot}}^{\mathrm{TS}} = E_{\mathrm{st}} + E_{\mathrm{dyn}}^{\mathrm{TS}}, \qquad (11)$$
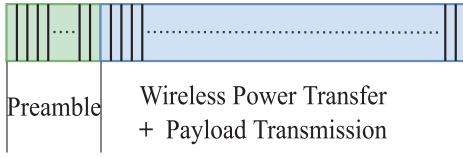
Fig. 6. Frame structure in the UC-splitting architecture.

Fig. 7. Post-preamble UC-splitting protocol functionality.

where E_{st} and E_{dyn}^{TS} denote the static and dynamic RIS energy consumption. Regarding E_{st}, it is expected to scale linearly with the number of UCs. Hence, by denoting the static power consumption per chip by P_{st}, it holds

$$E_{st} = M_s N_{fr} T_{sl} P_{st}. \tag{12}$$

As far as E_{dyn}^{TS} is concerned, by denoting the energy cost for a UC reconfiguration by E_{UC}, for the upper bound on E_{dyn}^{TS} per frame it holds

$$E_{dyn}^{TS} = N_{rec}^{TS} E_{UC} = E_{rec}^{CE} + E_{rec}^{PT} \\ + E_{rec}^{IT} = M_s (2\mu N_{pr} + 2) E_{UC}, \tag{13}$$

where $E_{rec}^{CE} = 2M_s \mu N_{pr} E_{UC}$ is the upper bound on the RIS energy consumption per frame related to channel estimation, $E_{rec}^{PT} = M_s E_{UC}$ is the RIS energy consumption per frame related to reconfiguration for power transfer, and $E_{rec}^{IT} = M_s E_{UC}$ is the RIS energy consumption per frame related to reconfiguration for information transmission. In practical scenarios it would hold that $\mu N_{pr} \gg 1$, which means that $E_{rec}^{CE} \gg E_{rec}^{PT} + E_{rec}^{IT}$. Consequently, the RIS energy consumption related to channel estimation is expected to be much higher than the required one for both reconfiguration for power transfer and information transmission. Finally, for the total energy consumption per frame in the time-splitting protocol, which we denote by E_{tot}^{TS}, it holds

$$E_{tot}^{TS} = E_{st} + E_{dyn}^{TS} = M_s (N_{fr} T_{sl} P_{st} + (2\mu N_{pr} + 2) E_{UC}). \tag{14}$$

2) Proposed UC-Splitting Protocol: The frame structure is depicted in Fig. 6. After the preamble transmission, simultaneous wireless power transfer and information transmission is realized by dedicating a subset of UCs for EH through perfect absorption and the rest for information transmission by acting as perfect reflectors and focusing towards the RX. The functionality of the RIS for the post-preamble frame interval is depicted in Fig. 7. In addition, in the UC-splitting protocol it holds that $N_{pt} = 0$. Hence,

$$N_{fr} = N_{pr} + N_{pl}. \tag{15}$$

Regarding the surface reconfigurations needed per frame, apart from the N_{rec}^{CE} reconfigurations needed for channel estimation, according to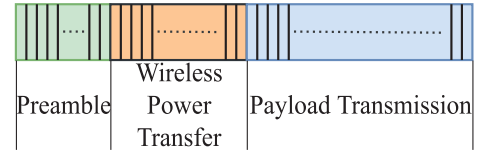 Fig. 6 additionally M_s reconfigurations are needed for adjusting the UC impedances for the simultaneous wireless power transfer and payload transmission interval. We denote the corresponding number of reconfigurations by N_{rec}^{PT+IT}. Hence, $N_{rec}^{PT+IT} = M_s$. As a result, the total number of surface reconfigurations per frame in the UC-splitting protocol, denoted by N_{rec}^{UC}, is given by

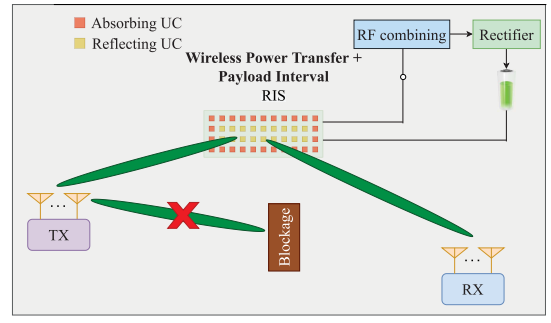$$N_{rec}^{UC} = N_{rec}^{CE} + N_{rec}^{PT+IT} = M_s (2\mu N_{pr} + 1). \tag{16}$$

Regarding the resulting dynamic energy consumption per frame, denoted by E_{dyn}^{UC}, it holds

$$E_{dyn}^{UC} = N_{rec}^{UC} E_{UC} = E_{rec} \\ + E_{rec}^{PT+IT} = M_s (2\mu N_{pr} + 1) E_{UC}, \tag{17}$$

where $E_{rec}^{PT+IT} = M_s E_{UC}$ is the energy consumption related to the M_s reconfigurations needed for simultaneous wireless power transfer and information transmission. As in the case of the time-splitting protocol, in practical scenarios it would hold that $E_{rec}^{CE} \gg E_{rec}^{PT+IT}$. Finally, the total energy consumption per frame, denoted by E_{tot}^{UC}, is given by

$$E_{tot}^{UC} = E_{st} + E_{dyn}^{UC} \\ = M_s (N_{fr} T_{sl} P_{st} + (2\mu N_{pr} + 1) E_{UC}). \tag{18}$$

3) Comparison With the Power-Splitting Protocol: As mentioned in Section I, a different approach to the UC-splitting protocol that can enable simultaneous energy harvesting and reflection for information transmission by the RIS is to allow all the UCs to be active and reflect only a part of the imping-ing to them electromagnetic energy. The remaining part can be absorbed and drive the EH circuits. This scheme is called power splitting. This possibility arises from the simultane-ous transmission and reflection (STAR)-RIS scheme where the power-splitting method allows a part of the impinging energy to be reflected by all the UCs and the rest to pass through the UCs and transmitted to the other side of the plane [24], [25].

Although this is a promising scheme, owing to the activation of all the UCs instead of only a subset of them, it is still at its infancy and only a very limited amount of prototypes and designs exist [26], [27], [28]. This is the reason why in this work we focus on the conventional time- and UC-splitting architectures. In terms of comparison with the UC-splitting protocol, the power-splitting protocol is expected to achieve a better SNR and resulting rate performance due to the fact that all the UCs are activated for reflection.

4) Complexity Comparison: Among the 3 presented har-vesting protocols, time-, UC-, and power-splitting, the easiest to implement is the UC-splitting protocol, since it is only based on dividing the UCs to the ones that only harvest energy and the ones that only reflect. On the other hand, the time-splitting protocol imposes very stringent time-synchronization require-ments due to the periodic switching between the absorption and reflection modes. Furthermore, the power-splitting proto-col requires a special design of the UCs so that they arbitrarily

adjust their reflection coefficient and at the same time reflect towards the desired location. Such a functionality cannot be achieved with conventional UCs [25].

C. Instantaneous SNR and Rate

1) SNR: The instantaneous end-to-end SNR related to the information transmission, denoted by γ, can be obtained by following the standard approach as [12], [29], [30], [31]

$$\gamma(\phi_k) = \frac{P_t}{\sigma^2} \left| \sum_{k \in \mathcal{A}_r} h_{t_k} h_{r_k} e^{j(\phi_k + \angle h_{t_k} + \angle h_{r_k})} \right|^2. \quad (19)$$

From (19) it is evident that the SNR is maximized by setting

$$\phi_k = -\angle h_{t_k} - \angle h_{r_k}, \text{ for } k \in \mathcal{A}_r. \quad (20)$$

By substituting (20) in (19), the maximum SNR can be written as

$$\gamma = \frac{P_t}{\sigma^2} \left(\sum_{k \in \mathcal{A}_r} |h_{t_k}| |h_{r_k}| \right)^2. \quad (21)$$

As stated in [12], we note that (20) indicates that independent tuning of the UC amplitude and phase response can be achieved. Although in general such independency does not hold [32], it could be achieved with advanced designs that mitigate such coupling [33], [34]. In this respect, (21) can be simply considered as an upper bound on the maximum achieved instantaneous SNR by advanced RIS designs.

2) Rate: Based on (21), the instantaneous rate, denoted by R, is given by

$$R = \frac{N_{\text{pl}}}{=} N_{\text{fr}} W \log_2(1 + \gamma) =$$

$$= \frac{N_{\text{pl}}}{N_{\text{fr}}} W \log_2 \left(1 + \frac{P_t}{\sigma^2} \left(\sum_{k \in \mathcal{A}_r} |h_{t_k}| |h_{r_k}| \right)^2 \right). \quad (22)$$

IV. PROBLEM FORMULATION AND SOLUTION

In this section, for both the time-splitting and UC-splitting cases the formulation of the problem of interest is presented and both analytical, that involve a single integral, and closed-form solutions are provided in the cases of random and deterministic TX-RIS channel gains, respectively.

A. Time-Splitting Protocol

We target the allocation of the resources in a way that the achievable average rate in a duration of a sufficiently large number of frames, denoted by K, is maximized. At the same time, the probability of the harvested energy, denoted by $E_{1 \to K}$, in the K-frame duration being smaller than the corresponding RIS energy consumption requirements should not exceed a threshold. It holds

$$E_{1 \to K} = \sum_{n=1}^{K} E_h = (N_{\text{fr}} - N_{\text{pr}} - N_{\text{pl}}) T_{\text{sl}} \sum_{n=1}^{K} P_{\text{DC}}(\mathcal{A}_s). \quad (23)$$

Problem A (Average Rate Maximization): This problem is formulated as

$$\underset{N_{\text{pl}}}{\text{maximize}} \quad \bar{R}^{(K)}(N_{\text{pl}})$$

$$\text{subject to} \quad \Pr\left\{ E_{1 \to K} \le K E_{\text{tot}}^{\text{fr}} \right\} \le \epsilon, \quad (24)$$

where ϵ is an outage probability threshold, $\bar{R}^{(K)}\{\cdot\}$ denotes the average rate value for the K-frame duration, and $\Pr\{\cdot\}$ denotes probability. We note that for sufficiently large K it holds that $\bar{R}^{(K)}(N_{\text{pl}}) \cong \bar{R}(N_{\text{pl}})$, where $\bar{R}(N_{\text{pl}})$ is the mean value of $R(N_{\text{pl}})$, due to the law of large numbers. Based on (22) and (23), (24) can be rewritten as

$$\underset{N_{\text{pl}}}{\text{maximize}} \quad N_{\text{pl}}$$

$$\text{subject to} \quad \Pr\left\{ \sum_{n=1}^{K} P_{\text{DC}}(\mathcal{A}_s) \le \frac{K E_{\text{tot}}^{\text{fr}}}{(N_{\text{fr}} - N_{\text{pr}} - N_{\text{pl}}) T_{\text{sl}}} \right\} \le \epsilon. \quad (25)$$

According to (25), we understand that the computation of the optimal value of N_{pl}, which we denote by N_{pl}^*, requires the knowledge of the cumulative density function (CDF) of $\sum_{n=1}^{K} P_{\text{DC}}(\mathcal{A}_s)$.

B. UC-Splitting Protocol

It holds

$$E_{1 \to K} = \sum_{n=1}^{K} E_h = (N_{\text{fr}} - N_{\text{pr}}) T_{\text{sl}} \sum_{n=1}^{K} P_{\text{DC}}(\mathcal{A}_h). \quad (26)$$

Problem B (Average Rate Maximization): The problem is formulated as

$$\underset{M_r}{\text{maximize}} \quad \bar{R}^{(K)}(M_r)$$

$$\text{subject to} \quad \Pr\left\{ E_{1 \to K} \le K E_{\text{tot}}^{\text{fr}} \right\} \le \epsilon. \quad (27)$$

Based on (22) and (26), (27) can be rewritten as

$$\underset{M_r}{\text{maximize}} \quad M_r$$

$$\text{subject to} \quad \Pr\left\{ \sum_{n=1}^{K} P_{\text{DC}}(\mathcal{A}_h) \le \frac{K E_{\text{tot}}^{\text{fr}}}{(N_{\text{fr}} - N_{\text{pr}}) T_{\text{sl}}} \right\} \le \epsilon. \quad (28)$$

According to (28), the computation of the optimal value of M_r, which we denote by M_r^*, requires the knowledge of the CDF of $\sum_{n=1}^{K} P_{\text{DC}}(\mathcal{A}_h)$. Hence, in both the time-splitting and UC-splitting protocols the computation of N_{pl}^* and M_r^* entails the computation of the CDF of $\sum_{n=1}^{K} P_{\text{DC}}(\mathcal{A}_h)$, where $\mathcal{A}_h \subseteq \mathcal{A}_s$.

Remark 2: In the case that $E_{1 \to K} > K E_{\text{tot}}^{\text{fr}}$, there can be different communication approaches. In particular, the RIS can be equipped with a battery that can be used in such situations. Another possibility could be to employ the accumulated energy surplus, considering that there is an overprovisioning in the allocation of the EH resources due to the consideration of the upper bound on $E_{\text{rec}}^{\text{CE}}$. Alternatively, the TX could switch to a sub-6 GHz band that is less susceptible to blockages compared

with mmWave bands and realize the communication with the RX without the involvement of an RIS.[7]

Furthermore, we note that the solution of (28) depends only on M_r and not on the particular selection of those UCs. This is due to the fact that the objective function in the problem is the average rate and not the instantaneous one. However, the particular selection of the UCs is expected to affect the radiation pattern of the RISs towards the RX, which might result in different interference levels in the case of neighbouring nodes that use the same frequency band. This is left as a topic for future work.

C. Computation of the CDF of $\sum_{n=1}^{K} P_{DC}(\mathcal{A}_h)$

Proposition 1: Let us denote the CDF of $\sum_{n=1}^{K} P_{DC}(\mathcal{A}_h)$ by $F_{DC}(x)$. $F_{DC}(x)$ is approximated by (29), shown at the bottom of the page, where $\phi_{h_t}(s)$ is the moment generating function (MGF) of $\sum_{n=1}^{K} P_{DC}(\mathcal{A}_h)$, given by (30), shown at the bottom of the page. $f_{h_t}(x)$ is the probability density function (pdf) of $\sum_{i \in \mathcal{A}_h} |h_{t_i}|^2$ and B, C, and G are constants. The range of values of B, C, and G for which $F_{DC}(x)$ is computed with a good accuracy depends on the statistics of $|h_{t_i}|$.[8]

Proof: See Appendix A. ∎

V. CHANNEL CASE STUDIES AND MONOTONIC TRENDS

The aim of this section is to show that $f_{h_t}(x)$ can be obtained in closed form for widely used indicative channel distributions that incorporate a strong LoS component together with multipath ones, such as the Rician and Nakagami-m ones. In addition, we prove monotonic trends of the ratio of the average achievable rates for the time- and UC-splitting protocols with respect to the RIS energy consumption in the case of optimal resource allocation.

Let us first assume that both the TX-RIS and RIS-RX links are subject to uncorrelated[9] fading. By considering for simplification a free-space propagation based path-loss exponent model[10] and by denoting the gains of TX antenna, RX antenna,

---

[7]This is in accordance with the fact that major telecom operators plan to use multiple bands for offering their 5G services [35].

[8]In [36] the authors find that the values $B = 18$, and $C = 24$, $G = 30$ give a good accuracy for Rician channels.

[9]This approximately holds only for d_{s_x} and d_{s_y} equal to half wavelength [37]. However, any correlation among the links can be readily incorporated into our framework according to the model of [37].

[10]In cases of dominant LoS components, the actual path-loss exponent is expected to be close to the free-space propagation one.

---

and each UC with $G_t(\theta)$, $G_r(\theta)$, and $G_s(\theta)$, respectively, it holds

$$\mathbf{h}_t = \begin{bmatrix} h_{t_1} \dots h_{t_{M_s}} \end{bmatrix}^T =$$
$$= \sqrt{\left(\frac{\lambda}{4\pi}\right)^2 \frac{G_t(\theta_{t,d}) G_s(\theta_{RIS,a})}{d_t^2}} \begin{bmatrix} \tilde{h}_{t_1} \dots \tilde{h}_{t_{M_s}} \end{bmatrix}^T \quad (31)$$

$$\mathbf{h}_r = \begin{bmatrix} h_{r_1} \dots h_{r_{M_s}} \end{bmatrix}^T =$$
$$= \sqrt{\left(\frac{\lambda}{4\pi}\right)^2 \frac{G_r(\theta_{r,a}) G_s(\theta_{RIS,d})}{d_r^2}} \begin{bmatrix} \tilde{h}_{r_1} \dots \tilde{h}_{r_{M_s}} \end{bmatrix}^T, \quad (32)$$

where λ is the wavelength. Furthermore, $\theta_{t,d}$, $\theta_{r,a}$, $\theta_{RIS,a}$, and $\theta_{RIS,d}$ denote the departure angle from the TX antenna, the arrival angle at the RX antenna, the arrival angle at the RIS, and the departure angle from the RIS, respectively.

A. Case Study: TX-RIS Links Subject to Rician Fading

It holds that:

$$\tilde{h}_{t_k} = e^{j\frac{2\pi}{\lambda} d_{t_k}} + m_k, \quad (33)$$

where $k = 1, 2, \dots, M_s$ and d_{t_k} is the distance between the TX and the center of the k_{th}. Furthermore, $m_k \in \mathcal{CN}(0, \sigma_t^2)$ represents the multipath complex envelopes of the Rayleigh fading that describes the diffuse scattering in the TX-RIS links.

Proposition 2: For the Rician fading case it holds that

$$f_{h_t}(x) = -\frac{b_{rice}^{M_h}(x)}{a_{rice}^{M_h-1}} e^{-\frac{\left(a_{rice}^2 + b_{rice}^2(x)\right)}{2}}$$
$$\times \frac{I_{M_h-1}(a_{rice} b_{rice}(x))}{2\sqrt{xP_t \frac{\sigma_t^2}{2} \frac{G_t(\theta_{t,d}) G_s(\theta_{RIS,a})}{d_t^2}}},$$
$$x > 0, \quad (34)$$

where

$$a_{rice} = \sqrt{\frac{2}{\sigma_t^2} M_h}, \quad b_{rice}(x) = \sqrt{\frac{x}{P_t \frac{\sigma_t^2}{2} \frac{G_t(\theta_{t,d}) G_s(\theta_{RIS,a})}{d_t^2}}}. \quad (35)$$

$I_{M_h-1}(\cdot)$ is the $(M_h - 1)$-th order modified Bessel function of the 1st kind.

Proof: See Appendix B. ∎

$$F_{DC}(x) \cong 2^{1-C} e^{A/2} \sum_{m=0}^{C} \binom{C}{m} \sum_{l=0}^{m+B} (-1)^l \alpha_l \mathbb{R}\left[\phi_{h_t}\left(\frac{G+j2\pi l}{2x}\right)/(G+j2\pi l)\right], \quad x > 0, \quad (29)$$

$$\phi_{h_t}(s) = \left[\frac{P_{max}\left(1 - \frac{1}{1+e^{ab}}\right)}{aP_t} \int_0^\infty \frac{e^{sx} f_{h_t}\left(\frac{1}{P_t}\left(-\frac{1}{a}\ln\left(\frac{P_{max}}{x\left(1-\frac{1}{1+e^{ab}}\right)+\frac{P_{max}}{1+e^{ab}}} - 1\right) + b\right)\right)}{\left(\frac{P_{max}}{x\left(1-\frac{1}{1+e^{ab}}\right)+\frac{P_{max}}{1+e^{ab}}} - 1\right)\left(x\left(1-\frac{1}{1+e^{ab}}\right)+\frac{P_{max}}{1+e^{ab}}\right)^2} dx\right]^K. \quad (30)$$

B. Case Study: TX-RIS Links Subject to Nakagami-m Fading

Let us assume that $\tilde{h}_{t_k}$, $k = 1, 2, \ldots, M_s$, is subject to Nakagami-m fading with fading severity parameter m_t and spread parameter σ_t^2.

Proposition 3: For the Nakagami-m fading case it holds that $f_{h_t}(x)$ is equal to (36), shown at the bottom of the page.

Proof: See Appendix C. ∎

C. Case Study: Deterministic TX-RIS Links

Proposition 4: In the case of deterministic TX-RIS links, such as the case of free-space propagation, for which $|h_{t_i}| = \sqrt{c}$, N_{pl}^* and M_r^* are given by

$$N_{\text{pl}}^* = \left\lfloor -\frac{1}{T_{\text{sl}}} \frac{E_{\text{tot}}^{\text{fr}}\left(1 - \frac{1}{1+e^{ab}}\right)}{\frac{P_{\max}}{1+e^{-a(P_t M_s c - b)}} - \frac{P_{\max}}{1+e^{ab}}} + N_{\text{fr}} - N_{\text{pr}} \right\rfloor \quad (37)$$

and

$$M_r^* = M_s - \left\lceil \left(\frac{1}{P_t c}\left(-\frac{1}{a}\ln\left(\frac{P_{\max}}{D} - 1 \right) + b \right) \right) \right\rceil, \quad (38)$$

where $D = \frac{E_{\text{tot}}^{\text{fr}}}{(N_{\text{fr}} - N_{\text{pr}})T_{\text{sl}}}\left(1 - \frac{1}{1+e^{ab}}\right) + \frac{P_{\max}}{1+e^{ab}}$.

Proof: Equations (37) and (38) originate by solving the constraints of (25) and (28) for $|h_{t_i}| = \sqrt{c}$. ∎

Remark 3: Based on (34) and (36), we see that $f_{h_t}(x)$ for well-known fading distributions that incorporate a LoS component, such as Rician and Nakagami-m, can be obtained in closed form. This means that the computation of (29) and, consequently, of N_{pl}^* and M_r^*, involves a single integral, which make them computationally efficient. In addition, the closed-form formulas (37) and (38) for the computation of N_{pl}^* and M_r^*, respectively, can be useful to the system designer in scenarios of highly directional transmissions and adequate elevations of the RIS. In such scenarios, it is expected that the TX-RIS links are subject only to very limited scattering, which means that the propagation characteristics for those links can approximately be described by the free-space propagation model.

D. Monotonic Trends for the Achievable Rate Ratio

We assume that K is adequately large so that $\bar{R}^{(K)} \cong \bar{R}$ holds, according to the law of large numbers. Let us now denote the achievable rates in the UC-splitting and time-splitting cases by $\bar{R}^{(\text{UC})}$ and $\bar{R}^{(T)}$, respectively. Before proceeding with the investigation of the monotonic trends of the ratio of the achievable rates of the two protocols, that we denote by ρ, let us first, without loss of generality, consider the Assumptions 1, 2, and 3 that follow, for simplifying the corresponding derivations.

Assumption 1: Both the TX-RIS and RIS-RX links are subject to free-space propagation. This means

$$h_{t_k} = \sqrt{\left(\frac{\lambda}{4\pi}\right)^2 \frac{G_t(\theta_{t,d})\,G_s(\theta_{\text{RIS,a}})}{d_t^2}} = \sqrt{c_t},$$

$$h_{r_k} = \sqrt{\left(\frac{\lambda}{4\pi}\right)^2 \frac{G_r(\theta_{r,a})\,G_s(\theta_{\text{RIS,d}})}{d_r^2}} = \sqrt{c_r}, \quad (39)$$

$k = 1, 2, \ldots, M_s$.

Assumption 2: The input power of the EH circuits is such that they operate in the region where the harvested power is an increasing function of the impinging RF power. In addition, we assume that the particular region can be approximated by a linear relationship between the input and harvested RF power.[11] In such a case, it approximately holds

$$P_{\text{DC}}(\mathcal{A}_h) \approx \eta P_{\text{RF}}(\mathcal{A}_h) = \eta P_t \sum_{i \in \mathcal{A}_h} |h_{t_i}|^2, \quad (40)$$

where η encompasses the RF-to-DC conversion efficiencies.

Assumption 3: $E_{\text{dyn}}^{\text{TS}}$, $E_{\text{dyn}}^{\text{UC}} \gg E_{\text{st}}$ holds. Consequently,

$$E_{\text{tot}}^{\text{TS}} \approx M_s(2\mu N_{\text{pr}} + 2)E_{\text{UC}}, \quad E_{\text{tot}}^{\text{UC}} \approx M_s(2\mu N_{\text{pr}} + 1)E_{\text{UC}}. \quad (41)$$

Based on the Assumptions 1, 2, and 3, ρ is given by

$$\rho = \frac{\bar{R}^{(\text{UC})}}{\bar{R}^{(T)}}$$
$$= \frac{(N_{\text{fr}} - N_{\text{pr}})\log_2\left(1 + (M_s - PE_{\text{UC}})^2 c_t c_r/\sigma^2\right)}{(-SE_{\text{UC}} + N_{\text{fr}} - N_{\text{pr}})\log_2(1 + M_s^2 c_t c_r/\sigma^2)}, \quad (42)$$

where

$$P = \frac{M_s(2\mu N_{\text{pr}} + 1)}{\eta c_t P_t(N_{\text{fr}} - N_{\text{pr}})T_{\text{sl}}} \approx \frac{2M_s\mu N_{\text{pr}}}{\eta c_t P_t(N_{\text{fr}} - N_{\text{pr}})T_{\text{sl}}},$$

$$S = \frac{2\mu N_{\text{pr}} + 2}{\eta c_t P_t T_{\text{sl}}} \approx \frac{2\mu N_{\text{pr}}}{\eta c_t P_t T_{\text{sl}}}. \quad (43)$$

The the approximations in (43) hold due to the fact that in practice it is expected that $\mu N_{\text{pr}} \gg 2 > 1$.

By considering Assumptions 1, 2, and 3 and by solving the constraints of (25) and (28), it holds

$$N_{\text{pl}}^* = -\frac{2\mu N_{\text{pr}} + 2}{\eta c_t P_t T_{\text{sl}}}E_{\text{UC}} + N_{\text{fr}} - N_{\text{pr}},$$

$$M_r^* = M_s - \frac{M_s(2\mu N_{\text{pr}} + 1)}{\eta c_t P_t(N_{\text{fr}} - N_{\text{pr}})T_{\text{sl}}}E_{\text{UC}}. \quad (44)$$

Lemma 1: The function $V(E_{\text{UC}}) = \frac{2M_s(N_{\text{fr}} - N_{\text{pr}} - SE_{\text{UC}})}{(N_{\text{fr}} - N_{\text{pr}})(M_s - PE_{\text{UC}})}$ is lower and upper bounded by 2 for $E_{\text{UC}} \in [0, E_{\text{th}})$, where

$$E_{\text{th}} = \frac{M_s}{P} = \frac{N_{\text{fr}} - N_{\text{pr}}}{S} = \frac{\eta c_t P_t(N_{\text{fr}} - N_{\text{pr}})T_{\text{sl}}}{2\mu N_{\text{pr}}} \quad (45)$$

[11] Such a region can occur for low input RF power [22, Fig. 2].

$$f_{h_t}(x) = \frac{1}{\Gamma(m_t M_h)}\left(\frac{m_t}{\sigma_t^2\left(\frac{\lambda}{4\pi}\right)^2 \frac{G_t(\theta_{t,d})\,G_s(\theta_{\text{RIS,a}})}{d_t^2}}\right)^{m_t M_h} x^{m_t M_h - 1} e^{-\frac{m_t x}{\sigma_t^2\left(\frac{\lambda}{4\pi}\right)^2 \frac{G_t(\theta_{t,d})\,G_s(\theta_{\text{RIS,a}})}{d_t^2}}}, \quad x > 0. \quad (36)$$

is the value of E_{UC} for which all the time and UC resources in the time-and UC-splitting cases, respectively, are dedicated to absorption and, hence, information transmission is not possible.

Proof: See Appendix D. ∎

Proposition 5: Under a high-SNR regime for the UC-splitting case ρ is a monotonically increasing function with respect to E_{UC}. On the other hand, in the low-SNR regime for the UC-splitting case, ρ is a monotonically decreasing function with respect to E_{UC}.

Proof: See Appendix E. ∎

Remark 4: Proposition 5 reveals that ρ has at least one local maximum in the range of E_{UC} for which the allocation of time and UC resources in the time- and UC-splitting cases, respectively, is feasible.

VI. NUMERICAL RESULTS

The aim of this section is threefold: i) to assess the gap in the achieved average rate performance between the time- and UC-splitting protocols, ii) to validate Proposition 5 and Remark 4, and iii) to show the importance of having analytical formulas for computing the optimal allocation of the harvesting resources in the examined protocols, based on (29). Towards this and without loss of generality, let us first make the assumptions of Sections VI-A and VI-B that follow, as a case study, regarding the geometrical arrangements together with the radiation patterns of the UCs and the TX and RX antennas.

A. Geometrical Arrangements

We assume that the planes of the TX and RX antennas are parallel to each other and the plane of the RIS is vertical to the TX and RX antenna planes. In addition, by $d_{t-r,h}$, $d_{t,h}$, $d_{t,v}$, $d_{r,v}$, h_t, h_r, and h_{RIS} we denote the horizontal TX-RX distance, the horizontal TX-RIS distance, the vertical TX-RIS distance, the vertical RIS-RX distance, the height of the TX, the height of the RX, and the height of the RIS, respectively. Then, it holds

$$d_t = \sqrt{d_{t,h}^2 + d_{t,v}^2 + (h_{\mathrm{RIS}} - h_t)^2},$$

$$d_r = \sqrt{\left(d_{t-r,h} - d_{t,h}\right)^2 + d_{r,v}^2 + (h_{\mathrm{RIS}} - h_r)^2}$$

$$\theta_{t,d} = \tan^{-1}\left(\frac{\sqrt{d_{t,v}^2 + (h_{\mathrm{RIS}} - h_t)^2}}{d_{t,h}}\right),$$

$$\theta_{r,a} = \tan^{-1}\left(\frac{\sqrt{d_{r,v}^2 + (h_{\mathrm{RIS}} - h_r)^2}}{|d_{t-r,h} - d_{t,h}|}\right)$$

$$\theta_{\mathrm{RIS,a}} = \frac{\pi}{2} - \theta_{t,d}, \quad \theta_{\mathrm{RIS,d}} = \frac{\pi}{2} - \theta_{r,a}. \tag{46}$$

B. TX/RX Antennas and UCs

By denoting the azimuth and elevation angles of the TX (RX) antenna by ϕ and θ, respectively, and assuming that the phase of its elements is adjusted so that the main lobe is directed to (θ_0, ϕ_0), for its directivity, which we denote by
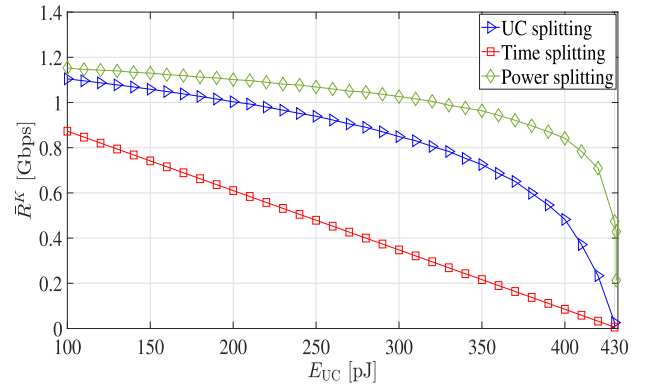

Fig. 8. *K*-frame average rate vs. the energy cost of a UC reconfiguration for $\sigma_t^2 = 0$.

$D_t(\theta, \phi)$ $(D_r(\theta, \phi))$, it holds [38]

$$D_t(\theta, \phi) = \frac{|g_t(\theta, \phi)|^2 |f(\theta, \phi)|^2}{M_{T_x} M_{T_y} R_t}, \tag{47}$$

where $g_t(\theta, \phi)$ and $f(\theta, \phi)$ are the array and element factors, respectively. Together with R_t they are given by [38]. For simplicity and without a loss of generality, in this work we consider the case of isotropic TX and RX antenna elements, i.e., $f(\theta, \phi) = 1$. Finally, the gains of the TX and RX antennas, which we denote by $G_t(\theta, \phi)$ and $G_r(\theta, \phi)$, respectively, are given by $G_t(\theta, \phi) = \epsilon_t D_t(\theta, \phi)$ and $G_r(\theta, \phi) = \epsilon_r D_r(\theta, \phi)$, where ϵ_t and ϵ_r are the efficiencies of the TX and RX antennas, respectively.

Furthermore, we consider that each UC exhibits a cosine gain pattern, with respect to the azimuth angle θ, expressed as [39]

$$G_s(\theta) = 4\cos(\theta), \quad 0 \leq \theta < \pi/2. \tag{48}$$

C. Simulation Results

Let us assume that both the TX-RIS and RIS-RX links are subject to Rician fading and that the received signal is subject to additive white complex Gaussian noise with power σ^2, computed in dBm as $\sigma^2 = -174 + 10\log_{10}(W) + \mathcal{F}_{\mathrm{dB}}$, where $\mathcal{F}_{\mathrm{dB}}$ is the noise figure of the RX in dB and W is the signal bandwidth in Hz. In addition, Table I presents the parameters used in the simulations, where σ_r^2 denotes the variance of the fast-fading complex envelope related to the RIS-RX links.

1) Evaluation of the Average Rate Performance: Fig. 8 depicts the average rate in the time- and UC-splitting cases versus E_{UC} for $\sigma_t^2 = 0$. Due to the fact that free-space propagation is assumed for the TX-RIS links ($\sigma_t^2 = 0$), N_{pl}^* and M_r^* for the time- and UC-splitting protocols are given by (37) and (38), respectively. We note that the maximum value $E_{\mathrm{UC}} = 432$ pJ for which we illustrate the results corresponds to the maximum possible allocation of resources for EH in both the time- and UC-splitting protocols (equal to 99% of available resources) for which information transmission is possible. As we observe, the UC-splitting protocol substantially outperforms its time-splitting counterpart throughout the depicted E_{UC} range. In particular, 4 and 6
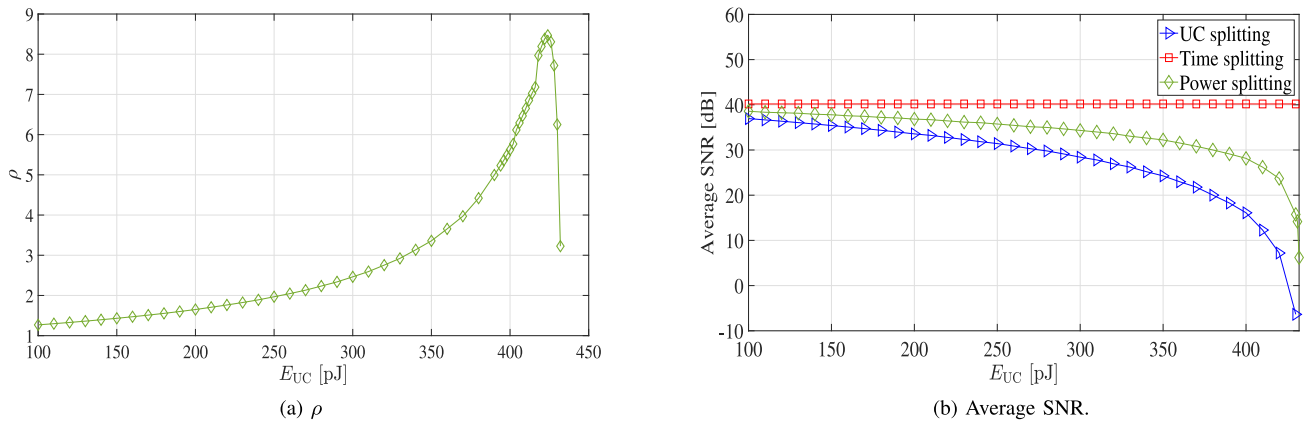
(a) ρ

(b) Average SNR.

Fig. 9. Average rate ratio (ρ) of the UC- over the time-splitting protocol and average SNR vs. the energy cost of a UC reconfiguration for $\sigma_t^2 = 0$.

TABLE I
PARAMETER VALUES USED IN THE SIMULATION

Parameter	Value	Parameter	Value
f	28 GHz	$d_{T_x}, d_{R_x}, d_{s_x}$ $d_{T_y}, d_{R_y}, d_{s_y}$	$\lambda/2$
M_{s_x}, M_{s_y}	15	e_t, e_r	0.9
P_t	1 W	σ_r^2	0.3
M_{T_x}, M_{T_y}	50	M_{R_x}, M_{R_y}	10
$d_{t-r,h}$	90 m	$T_{\rm sl}$	1 μs
$d_{t,h}$	15 m	$d_{t,v}$	6 m
$d_{r,v}$	10 m	h_t, h_r	3 m
$h_{\rm RIS}$	12 m	$N_{\rm pr}$	10^3
$\mathcal{F}_{\rm dB}$	10 dB	a	120
b	10^{-3}	$P_{\max}$	20 mW
W	100 MHz	ϵ	10^{-2}
$P_{\rm st}$	1 μW	K	10^4
μ	0.2	$N_{\rm fr}$	10^4

times higher average rate is achieved for $E_{\rm UC} = 350$ and $E_{\rm UC} = 400$ pJ, respectively. Moreover, a notable trend we observe is that the rate decrease with respect to an increasing $E_{\rm UC}$ is more pronounced in the time-splitting protocol case up to a certain $E_{\rm UC}$ value, whereas it becomes more pronounced in the UC-splitting case close to the maximum possible $E_{\rm UC}$ value. In addition, in Fig. 9 we also plot the average rate performance of the power-splitting protocol that we mentioned in Section III-B3. As we observe, it achieves a higher performance than the UC-splitting protocol as expected according to the intuition presented in Section III-B3.

2) Validation of Proposition 5 and Remark 4: The aforementioned rate trend with respect to $E_{\rm UC}$ for the time- and UC-splitting protocols is further substantiated in Fig. 9 that illustrates the ratio ρ of the average rate of the UC-splitting protocol over the corresponding one of the time-splitting protocol together with the average SNR versus $E_{\rm UC}$ for $\sigma_t^2 = 0$. As far as ρ is concerned, in Fig. 9-(a) two regions are distinguished. In the 1st region the ratio is a monotonically increasing function until a peak is reached after which the ratio becomes a monotonically decreasing function with respect to $E_{\rm UC}$. The latter region starts occurring close to the maximum value of $E_{\rm UC}$, where the average rate of the UC-splitting protocol starts decreasing rapidly. To verify that the

monotonically increasing and decreasing regions correspond to the high-SNR and low-SNR regimes, respectively, of the UC-splitting protocol, based on Proposition 5, in Fig. 9-(b) we depict the average achieved SNR vs. $E_{\rm UC}$ for $\sigma_t^2 = 0$. As we observe from Fig. 9-(b), in the monotonically increasing region the SNR in the UC-splitting case stays above 10 dB, whereas it is below the particular value in the monotonically decreasing one. Hence, these regions respectively correspond to the high- and low-SNR region for the UC-splitting case, which validates Proposition 5. In addition, the unique local maximum observed (consequently, a global maximum), validates Remark 4. Finally, for illustrative reasons, in Fig. 9-(b) we also depict the average SNR achieved by the power-splitting protocol. We observe that the particular protocol achieves a higher SNR than its UC-splitting counterpart, which again verifies the intuitive comment on such a performance comparison of Section III-B3.

Now that the expected monotonic trends from Proposition 5 have been validated, let us provide an intuitive explanation of why ρ monotonically increases in the high-SNR and decreases in the low-SNR region of the UC-splitting protocol. These trends are justified by the fact that in the time-splitting case the factor corresponding to the reduction of time resources for an increasing $E_{\rm UC}$, that are dedicated to information transmission, is a multiplicative factor of the logarithm function in (24). Hence, there is a linear decrease of the average rate in the time-splitting case throughout the $E_{\rm UC}$ range. On the other hand, for the UC-splitting protocol case such a term is included inside the logarithm function in (27), which justifies the smaller slope in the average rate reduction in the high-SNR region, as depicted in Fig. 8. In turn, this results in a monotonically increasing behavior of ρ in the particular region. On the other hand, in the low-SNR region for the UC-splitting protocol it holds that $\log 2(1 + \gamma) \approx \log 2(e)\gamma$ for $\gamma \ll 1$. In addition, the SNR reduction in the UC-splitting case scales quadratically with $E_{\rm UC}$, as the factor $(M_s - PE_{\rm UC})^2 c_t c_r / \sigma^2$ in the proof of Proposition 5 reveals for the low-SNR region. Consequently, in the low-SNR region for the UC-splitting case ρ involves the ratio of a term that quadratically reduces with $E_{\rm UC}$ over a term that linearly reduces with $E_{\rm UC}$. This justifies the monotonic decrease of ρ.

(a) Time-splitting protocol.

(b) UC-splitting protocol.
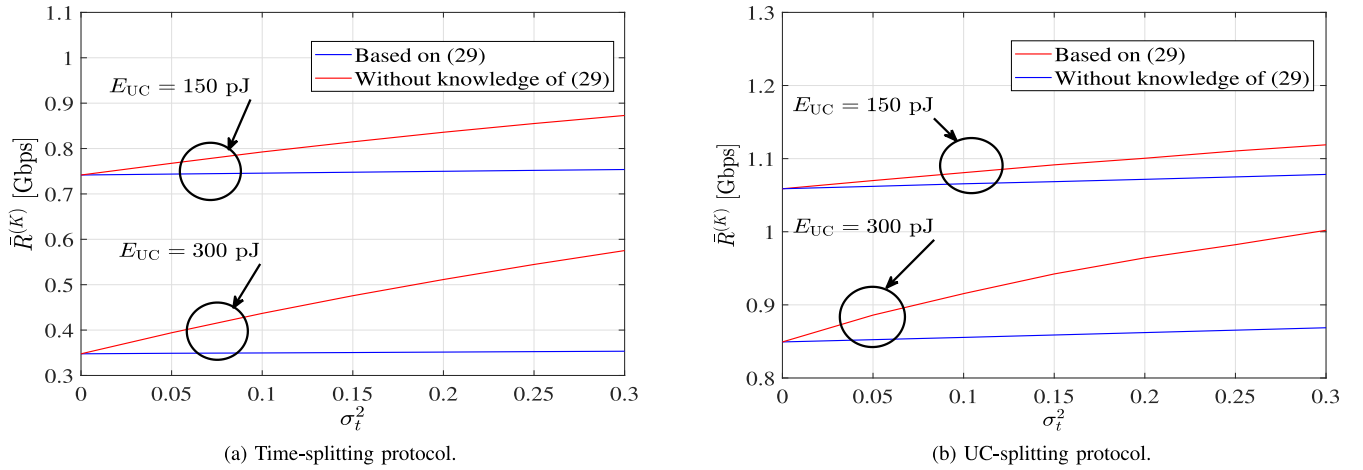
Fig. 10. $\bar{R}^{(K)}$ vs. σ_t^2.

3) Importance of the Analytical Framework of (29)*:* In the case that the analytical framework of (29) is absent, the only possibility for resource allocation is to perform over-provisioning and allocate the resources only based on the knowledge of the impinging strength of the LoS component. Fig. 10 reveals how suboptimal such an approach is for the time- and UC-splitting protocols and for 2 values of E_{UC}. As we observe from Fig. 10, the higher σ_t^2 is the higher the achieved rate gain is by the knowledge of the analytical framework. This was expected since higher values of σ_t^2 mean that additional power is delivered to the RIS compared with having only the LoS component. Consequently, notably less resources for energy harvesting need to be dedicated. Moreover, the rate gain increases with increasing E_{UC}. In particular, for $E_{\text{UC}} = 300$ pJ and $\sigma_t^2 = 0.3$ we observe that the rate gain by having the analytical framework is around 63% and 15.3% in the time- and UC-splitting cases, respectively.

Remark 5: By observing Fig. 8, the intuitive decision regarding which of the time- and UC-splitting protocols should be selected would be the UC-splitting one since it substantially outperforms its time-splitting counterpart throughout the E_{UC} range. However, such a decision does not consider a possible constraint on the required SNR to achieve a target error rate. In particular, for higher E_{UC} values than the one achieving the peak in the ρ vs. E_{UC} curve of Fig. 9-(a) we see from Fig. 9-(b) that the average SNR in the UC-splitting case rapidly falls for slight increases of E_{UC}. Hence, the existence of such a peak and the very rapid drop of the UC-splitting case SNR beyond the peak gives information to the system designer to design RIS electronics that exhibit a power consumption that allows the RIS to operate below the rapidly falling region regarding the SNR in the UC-splitting case. In such a case the UC-splitting protocol would be the best choice. In addition, as a safety margin, it would be desirable that the power consumption of the RIS electronics is such that such operation is not close to the particular region. Such a margin is desirable for the following two reasons: i) Over the years the energy consumption of electronics is naturally expected to increase, which means that a small margin between the operation point and the rapidly falling SNR region would pose a risk. ii) Even if E_{UC} ideally remains steady over the years, the

same effect in the total RIS energy consumption of increasing E_{UC} can be exerted by an increase of μ, based on (13). Such an increase of μ might occur due to a change of the sparsity level of the TX-RIS links. In particular, under a reduction of the channel sparsity level it would be expected that μ increases in order to maintain the reliability level of the channel estimation. This, in turn, would increase the RIS energy consumption and drive the operating region in the UC-splitting protocol closer or even inside the rapidly falling region of the SNR. Consequently, if such a desirable sufficient margin cannot be achieved, the best choice would be the time-splitting protocol in which the SNR remains unaffected by the RIS energy consumption. Even though such a choice would lead to a lower achievable rate compared to the UC-splitting protocol, it would be the best choice so to avoid an SNR drop below what would be considered as acceptable, related to the application.

Remark 6: Based on the parameter values of Table I, it holds that $E_{\text{dyn}}^{\text{TC}}$, $E_{\text{dyn}}^{\text{UC}} \gg E_{\text{st}}$. This is expected in future practical cases since the static power consumption of RIS electronics, depending on the technology used, is expected to be small, especially if asynchronous logic is considered [40]. Although the resulting static power consumption of the considered electronic chips in [40] is higher than what can be supplied wirelessly by information signals, this is only the first family of application-specific integrated circuits suitable to the integrated architecture that is considered as the most viable approach for autonomous RISs [4], [5], [6]. Hence, in the years to come many advances are expected regarding the design of circuits that would exhibit a lower static power consumption.

4) Impact of the Preamble Length on the Performance: Let us now examine how the length of the preamble interval, where channel estimation is performed, impacts the individual performance of the time- and UC-splitting protocols and also the performance gap between them. Towards this, firstly in Fig. 11 we depict the normalized mean-square error (NMSE) related to the estimation of the cascaded TX-RIS-RX channel, based on [18], vs. N_{pr} for $E_{\text{UC}} = 300$ pJ. As we observe from Fig. 11, the NMSE rapidly drops until $N_{\text{pr}} = M_s$ and then it slowly reduces. This is justified by the lack of sparsity in the RIS-RX channel, since independent and identical
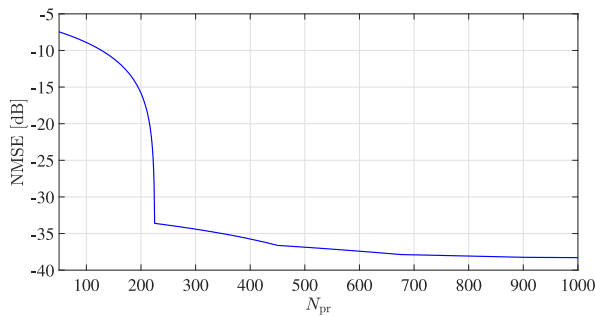
Fig. 11.   NMSE vs. N_{pr} for $E_{\mathrm{UC}} = 300$ pJ.

distributed fading is assumed for the scattered component of the Rician process. Hence, if $N_{\mathrm{pr}} < M_s$, the channel value that we used for the remaining $N_{\mathrm{pr}} - M_s$ TX-RIS-RX links that channel estimation cannot be performed is the value of the LoS component. This is the component that is not subject to channel estimation since it can be calculated solely by the geometrical arrangements of the TX, RIS, and RX. As a result, by replacing those values with the ones that result from the estimation of the scattered component as well, the NMSE rapidly improves, which justifies the sudden drop of NMSE in the $N_{\mathrm{pr}} < M_s$ region as N_{pr} increases.

Finally, in Fig. 12 we depict the average rate and SNR curves for the time-and UC-splitting protocols vs. N_{pr}. As we observe, in terms of average rate the gap between the 2 protocols increases with N_{pr} due to the fact that the reduction of the resources with respect to an increasing N_{pr} is a multiplicative factor of the logarithm function in the time-splitting case, whereas it is a factor inside the logarithm function in the UC-splitting case. In terms of average SNR Fig. 12-(b) reveals that there is only a small impact with respect to the lack of knowledge of the scattered component of the RIS-RX channel in the case of small N_{pr}. This can be understood by the fact that the average SNR in the time-splitting case only slightly increases with the increase of N_{pr} in the $N_{\mathrm{pr}} < M_s$ region, as we observe. This is a clear indication of the importance of the dominant LoS component over the scattered one.

VII. CONCLUSION

We have conducted this work to give an answer to system designers of whether a time-splitting or a UC-splitting protocol for autonomous RIS operation is more beneficial in terms of average rate. Towards the aforementioned goal, we have proposed two realistic frame structures for the considered protocols and computed the RIS energy consumption demands per frame that take into account the energy burden for channel estimation. In addition, for both proposed protocols we have considered low-complexity offline schemes for the optimal allocation of resources for EH, based on long-term statistics, that involve the average rate maximization while meeting the long-term RIS energy consumption demands. A closed-form solution was provided in the case of deterministic channel gains for the TX-RIS links and single-integral easy-to-compute expressions for the case of Rician and Nakagami-m channels. In addition, we have proved that the ratio of the average rate of the UC-splitting case over its time-splitting counterpart exhibits a monotonically increasing behavior with

respect to the energy consumption for a UC reconfiguration in the region of high SNR for the UC-splitting protocol. On the other hand, in the low-SNR region the ratio is steeply monotonically decreasing together with the corresponding SNR of the UC-splitting protocol.

Such an outcome, which has been validated by means of simulations, gives the important information to system designers that the choice of the UC-splitting protocol is preferable in the region of high-SNR operation, provided that the operation point is sufficiently far from the transition point between the two regions. On the other hand, if the energy consumption for a UC reconfiguration is such that the operation point in the UC-splitting case is close to the transition point, it would be preferable to choose the time-splitting protocol in which the SNR does not depend on such a consumption, even though the latter protocol exhibits a lower average rate. This is in order to prevent a rapid fall of the SNR that would be observed in the case of the UC-splitting protocol for even slight increases in the RIS energy consumption that may occur. Such increases might be due to unexpected changes in the channel statistics or aging of the RIS electronics. Finally, we have substantiated the analytical framework importance for the computation of the optimal allocation of the EH resources in the case of generic fading channels. Notable rate gains were observed compared with the case of over-provisioning the resources due to the lack of such a framework. Future work will consider the analytical performance comparison of the UC- and power-splitting protocols.

APPENDIX A
PROOF OF PROPOSITION 1

By assuming that the channel gains among different frames are independent, $\sum_{n=1}^{K} P_{\mathrm{DC}}(\mathcal{A}_h)$ consists of the summation of K independent random variables following the same distribution. Hence,
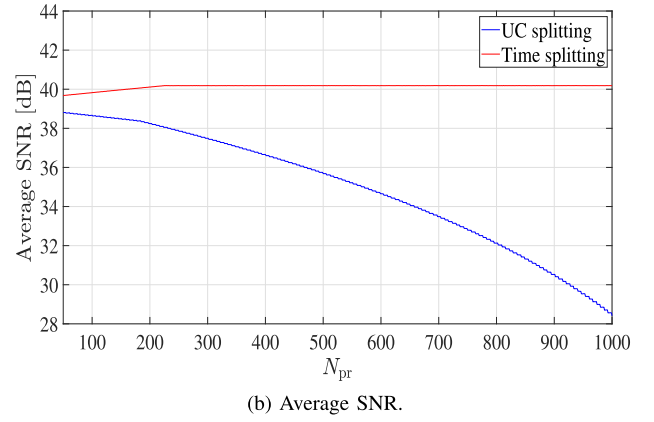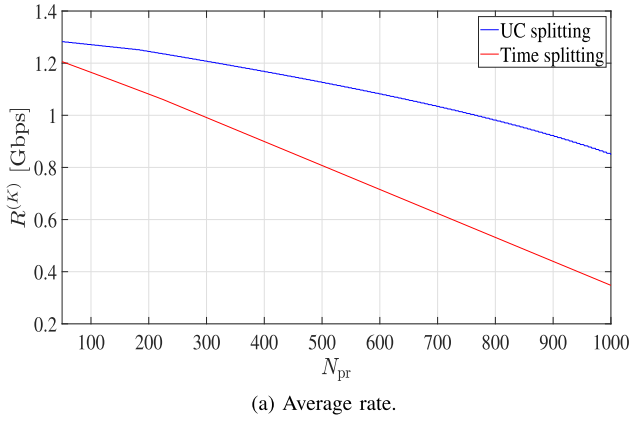
$$\phi_{h_t}(s) = \left[\int_0^\infty e^{sx} h_{\mathrm{DC}}(x) \right]^K, \qquad (49)$$

where $h_{\mathrm{DC}}(x)$ is the pdf of $P_{\mathrm{DC}}(\mathcal{A}_h)$. Based on (5) the CDF of $P_{\mathrm{DC}}(\mathcal{A}_h)$, which we denote by $H_{\mathrm{DC}}(x)$, is given by (50), shown at the bottom of the next page. By taking the first derivative of $H_{\mathrm{DC}}(x)$ and plugging it into (49), (30) is obtained. Finally, by employing the Laplace inversion method detailed in [41, Eq. (6)] and by truncating the resulting infinite series, (29) is obtained.

APPENDIX B
PROOF OF PROPOSITION 2

For the CDF of $\sum_{i \in \mathcal{A}_h} |h_{t_i}|^2$, which we denote by $F_{h_t}(x)$, it holds

$$F_{h_t}(x) = P_r \left\{ \sum_{i \in \mathcal{A}_h} |h_{t_i}|^2 \le x \right\}$$

$$= P_r \left\{ \sum_{i \in \mathcal{A}_h} \left(\frac{\lambda}{4\pi} \right)^2 \frac{G_t G_s(\theta_{\mathrm{inc}})}{d_t^2} \left| \tilde{h}_{t_i} \right|^2 \le x \right\}$$

(a) Average rate.

(b) Average SNR.

Fig. 12. Average rate and SNR vs. N_{pr} for $E_{\text{UC}} = 300$ pJ.

$$= P_r \left\{ \sum_{i=1}^{2M_h} \left| \tilde{h}'_{t_i} \right|^2 \leq \frac{x}{\left(\frac{\lambda}{4\pi}\right)^2 \frac{G_t G_s(\theta_{\text{inc}})}{d_t^2} \frac{\sigma_t^2}{2}} \right\}$$

$$\stackrel{(a)}{=} 1 - Q_{M_h}(a_{\text{rice}}, b_{\text{rice}}(x)), \quad (51)$$

where $Q_{M_h}(\cdot, \cdot)$ is the generalized Marcum Q-function of order M_h. (a) arises due to the fact that $\sum_{i=1}^{2M_h} |\tilde{h}'_{t_i}|^2$ consists of the summation of the squares of $2M_h$ independent, normally distributed random variables, with means equal to $\frac{2}{\sigma_t^2}(\Re\{e^{j\frac{2\pi}{\lambda} d_{t_i}}\})^2$, $\frac{2}{\sigma_t^2}(\Im\{e^{j\frac{2\pi}{\lambda} d_{t_i}}\})^2$ and unit variances.[12] Hence, $\sum_{i=1}^{2M_h} |\tilde{h}'_{t_i}|^2$ follows a non-central chi-squared distribution with $2M_h$ degrees of freedom and mean parameter equal to $(\frac{2}{\sigma_t^2})\sum_i^{M_h}(\Re\{e^{j\frac{2\pi}{\lambda} d_{t_i}}\})^2 + (\Im\{e^{j\frac{2\pi}{\lambda} d_{t_i}}\})^2 = (\frac{2}{\sigma_t^2})M_h$. Finally, by taking the 1st derivative of $F_{h_t}(x)$ with respect to x and using [42, eq. (13)], (34) is obtained.

APPENDIX C
PROOF OF PROPOSITION 3

For the CDF of $\sum_{i \in \mathcal{A}_h} |h_{t_i}|^2$, denoted by $F_{h_t}(x)$, it holds that $F_{h_t}(x)$ is equal to (52), shown at the bottom of the page, where $\gamma(\cdot, \cdot)$ is the lower incomplete gamma function. (b) arises by considering that the square of a Nakagami-m random variable is Gamma distributed with shape m_t and scale σ_t^2/m_t and the summation of M_h uncorrelated Gamma variables having the same scale is also Gamma distributed with shape equal

[12]The independence property comes from the fact that uncorrelated normal variables are also independent variables.

to $m_t M_h$ and scale equal to σ_t^2/m_t [43]. Finally, (36) results from the 1st derivative of $F_{h_t}(x)$ from (52).

APPENDIX D
PROOF OF LEMMA 1

It holds that

$$V(0) = 2,$$

$$V(E_{\text{th}}) \stackrel{(c)}{=} \frac{2M_s \lim_{E_{\text{UC}} \to E_{\text{th}}} \frac{d(N_{\text{fr}} - N_{\text{pr}} - SE_{\text{UC}})}{dE_{\text{UC}}}}{(N_{\text{fr}} - N_{\text{pr}}) \lim_{E_{\text{UC}} \to E_{\text{th}}} \frac{d(M_s - PE_{\text{UC}})}{dE_{\text{UC}}}} = 2,$$
$$(53)$$

where (c) is due to the L'hospital's rule. In addition, it holds that $\frac{dV(E_{\text{UC}})}{dE_{\text{UC}}} = 0$, which means that $V(E_{\text{UC}})$ is lower and upper bounded by the number 2 for $E_{\text{UC}} \in [0, E_{\text{th}}]$, taking also into account (53).

APPENDIX E
PROOF OF PROPOSITION 5

1) High-SNR Region: It suffices to prove that $d\rho/dE_{\text{UC}} > 0$ for $(M_s - PE_{\text{UC}})^2 c_t c_r/\sigma^2 \gg 1$ (high-SNR region in the UC-splitting case). Let us now test the hypothesis $d\rho/dE_{\text{UC}} > 0$. It holds that

$$d\rho/dE_{\text{UC}} > 0 \stackrel{(d)}{\Rightarrow}$$

$$\ln\left((M_s - PE_{\text{UC}})^2 c_t c_r/\sigma^2\right) > V(E_{\text{UC}}) \stackrel{(e)}{=} 2 \quad \text{true,} \quad (54)$$

where in (d) we use the approximation

$$1 + (M_s - PE_{\text{UC}})^2 c_t c_r/\sigma^2 \approx (M_s - PE_{\text{UC}})^2 c_t c_r/\sigma^2 \quad (55)$$

$$H_{\text{DC}}(x) = P_r\{P_{\text{DC}}(\mathcal{A}_h) \leq x\} = P_r\left\{ \sum_{i \in \mathcal{A}_h} |h_{t_i}|^2 \leq \frac{1}{P_t}\left(-\frac{1}{a} \ln\left(\frac{P_{\max}}{x\left(1 - \frac{1}{1+e^{ab}}\right) + \frac{P_{\max}}{1+e^{ab}}} - 1 \right) + b \right) \right\}. \quad (50)$$

$$F_{h_t}(x) = P_r\left\{ \sum_{i \in \mathcal{A}_h} |h_{t_i}|^2 \leq x \right\} = P_r\left\{ \sum_{i=1}^{M_h} |\tilde{h}_{t_i}|^2 \leq \frac{x}{\left(\frac{\lambda}{4\pi}\right)^2 \frac{G_t G_s(\theta_{\text{inc}})}{d_t^2}} \right\} \stackrel{(b)}{=} \frac{1}{\Gamma(m_t M_h)} \gamma\left(m_t M_h, \frac{m_t x}{\sigma_t^2 \left(\frac{\lambda}{4\pi}\right)^2 \frac{G_t G_s(\theta_{\text{inc}})}{d_t^2}} \right) \quad (52)$$

$$d\rho/dE_{\mathrm{UC}} < 0 \Rightarrow \ln\Big(1 + (M_s - PE_{\mathrm{UC}})^2 c_t c_r/\sigma^2\Big)\Big(1 + (M_s - PE_{\mathrm{UC}})^2 c_t c_r/\sigma^2\Big)$$
$$> 2\frac{M_s}{N_{\mathrm{fr}} - N_{\mathrm{pr}}}(M_s - PE_{\mathrm{UC}})(N_{\mathrm{fr}} - N_{\mathrm{pr}} - SE_{\mathrm{UC}})c_t c_r/\sigma^2 \overset{(f)}{\Rightarrow} 1 < V(E_{\mathrm{UC}}) \quad \text{true,} \tag{56}$$

$$1 + (M_s - PE_{\mathrm{UC}})^2 c_t c_r/\sigma^2 \approx 1, \quad \ln\Big(1 + (M_s - PE_{\mathrm{UC}})^2 c_t c_r/\sigma^2\Big) \approx (M_s - PE_{\mathrm{UC}})^2 c_t c_r/\sigma^2. \tag{57}$$

and in (*e*) Lemma 1. The last inequality of (54) holds, which validates the hypothesis, due to the fact that it is expected that $\ln((M_s - PE_{\mathrm{UC}})^2 c_t c_r/\sigma^2) > 2$ in the high-SNR region $((M_s - PE_{\mathrm{UC}})^2 c_t c_r/\sigma^2 \gg 1)$.

2) Low-SNR Region: It suffices to prove that $d\rho/dE_{\mathrm{UC}} < 0$ for $(M_s - PE_{\mathrm{UC}})^2 c_t c_r/\sigma^2 \ll 1$ (low-SNR region in the UC-splitting case), which holds as shown in (56), at the top of the page, where in (*f*) we use the approximations in (57), shown at the top of the page. The last inequality of (56) holds, which validates the hypothesis, due to Lemma 1. Based on (54) and (56), the proof of Proposition 5 has been concluded.

REFERENCES

[1] M. Di Renzo et al., "Smart radio environments empowered by reconfigurable intelligent surfaces: How it works, state of research, and the road ahead," *IEEE J. Sel. Areas Commun.*, vol. 38, no. 11, pp. 2450–2525, Nov. 2020.

[2] E. Björnson, Ö. Özdogan, and E. G. Larsson, "Reconfigurable intelligent surfaces: Three myths and two critical questions," *IEEE Commun. Mag.*, vol. 58, no. 12, pp. 90–96, Dec. 2020.

[3] "Industry specification group (ISG) on reconfigurable intelligent surfaces (RISs)." Accessed: Mar. 24, 2023. [Online]. Available: https://www.etsi.org/committee-activity/activity-report-ris

[4] S. Abadal, T. Cui, T. Low, and J. Georgiou, "Programmable metamaterials for software-defined electromagnetic control: circuits, systems, and architectures," *IEEE J. Emerg. Sel. Topics Power Electron.*, vol. 10, no. 1, pp. 6–19, Mar. 2020.

[5] A. C. Tasolamprou et al., "Exploration of intercell wireless millimeter-wave communication in the landscape of intelligent metasurfaces," *IEEE Access*, vol. 7, pp. 122931–122948, Aug. 2019.

[6] C. Liaskos, S. Nie, A. Tsioliaridou, A. Pitsillides, S. Ioannidis, and I. Akyildiz, "Realizing wireless communication through software-defined hypersurface environments," in *Proc. IEEE 19th Int. Sympo. World Wireless Mobile Multimedia Netw. (WoWMoM)*, 2018, pp. 14–15.

[7] Y. Zou, S. Gong, J. Xu, W. Cheng, D. T. Hoang, and D. Niyato, "Wireless powered intelligent reflecting surfaces for enhancing wireless communications," *IEEE Trans. Veh. Technol.*, vol. 69, no. 10, pp. 12369–12373, Oct. 2020.

[8] Z. Chu, P. Xiao, D. Mi, W. Hao, M. Khalily, and L.-L. Yang, "A novel transmission policy for intelligent reflecting surface assisted wireless powered sensor networks," *IEEE J. Sel. Topics Signal Process.*, vol. 15, no. 5, pp. 1143–1158, Aug. 2021.

[9] S. Hu, Z. Wei, Y. Cai, C. Liu, D. W. K. Ng, and J. Yuan, "Robust and secure sum-rate maximization for multiuser MISO downlink systems with self-sustainable IRS," *IEEE Trans. Commun.*, vol. 69, no. 10, pp. 7032–7049, Oct. 2021.

[10] Y. Pan, K. Wang, C. Pan, H. Zhu, and J. Wang. "Self-sustainable reconfigurable intelligent surface aided simultaneous terahertz information and power transfer (STIPT)." Accessed: Mar. 24, 2023. [Online]. Available: https://arxiv.org/abs/2102.04053

[11] K. Ntontin et al., "Autonomous reconfigurable intelligent surfaces through wireless energy harvesting," in *Proc. IEEE 95th VTC Spring*, Jun. 2022, pp. 1–6.

[12] K. Ntontin et al., "Wireless energy harvesting for autonomous reconfigurable intelligent surfaces," *IEEE Trans. Green Commun. Netw.*, vol. 7, no. 1, pp. 114–129, Mar. 2023.

[13] B. Lyu, P. Ramezani, D. T. Hoang, S. Gong, Z. Yang, and A. Jamalipour, "Optimized energy and information relaying in self-sustainable IRS-empowered WPCN," *IEEE Trans. Commun.*, vol. 69, no. 1, pp. 619–633, Jan. 2021.

[14] K. Ntontin, A. A.-A. Boulogeorgos, Z. Abdullah, A. Mesodiakaki, S. Abadal, and S. Chatzinotas, "Time vs. Unit cell splitting for autonomous reconfigurable intelligent surfaces," in *Proc. IEEE GLOBECOM*, 2022, pp. 3332–3337.

[15] I. A. Hemadeh, K. Satyanarayana, M. El-Hajjar, and L. Hanzo, "Millimeter-wave communications: Physical channel models, design considerations, antenna constructions, and link-budget," *IEEE Commun. Surveys Tuts.*, vol. 20, no. 2, pp. 870–913, 2nd Quart., 2018.

[16] E. Arslan, I. Yildirim, F. Kilinc, and E. Basar, "Over-the-air equalization with reconfigurable intelligent surfaces," *IET Commun.*, vol. 16, no. 13, pp. 1486–1497, 2022.

[17] D.-W. Yue, Y. Zhang, and Y. Jia, "Beamforming based on specular component for massive MIMO systems in Ricean fading," *IEEE Wireless Commun. Lett.*, vol. 4, no. 2, pp. 197–200, Apr. 2015.

[18] Z.-Q. He and X. Yuan, "Cascaded channel estimation for large intelligent metasurface assisted massive MIMO," *IEEE Wireless Commun. Lett.*, vol. 9, no. 2, pp. 210–214, Feb. 2020.

[19] W. Tang et al., "On channel reciprocity in reconfigurable intelligent surface assisted wireless network," 2021, *arXiv:2103.03753*.

[20] A. Jiménez-Sáez, A. Asadi, R. Neuder, D. Wang, and R. Jakoby, "Liquid crystals: The way to scalable and practical reconfigurable intelligent surfaces in 6G," Oct. 2022. [Online]. Available: https://www.techrxiv.org/articles/preprint/Liquid_Crystals_The_way_to_Scalable_and_Practical_Reconfigurable_Intelligent_Surfaces_in_6G/21335733

[21] D. Altinel and G. K. Kurt, "Diversity combining for RF energy harvesting," in *Proc. IEEE 85th VTC Spring*, 2017, pp. 1–5.

[22] E. Boshkovska, D. W. K. Ng, N. Zlatanov, and R. Schober, "Practical non-linear energy harvesting model and resource allocation for SWIPT systems," *IEEE Commun. Lett.*, vol. 19, no. 12, pp. 2082–2085, Dec. 2015.

[23] "Report on the comparison between ideal hypersurface (HSF)s and the manufactured prototypes, VISORSURF project." Dec. 2020. [Online]. Available: https://ec.europa.eu/research/participants/documents/downloadPublic?documentIds=080166e5d7993c7d&appId=PPGMS

[24] Y. Liu et al., "STAR: Simultaneous transmission and reflection for 360° coverage by intelligent surfaces," *IEEE Wireless Commun.*, vol. 28, no. 6, pp. 102–109, Dec. 2021.

[25] J. Xu, Y. Liu, X. Mu, and O. A. Dobre, "STAR-RISs: Simultaneous transmitting and reflecting reconfigurable intelligent surfaces," *IEEE Wireless Commun. Lett.*, vol. 25, no. 9, pp. 3134–3138, Sep. 2021.

[26] N. Docomo. "DOCOMO conducts world's first successful trial of transparent dynamic metasurface." Accessed: Mar. 24, 2023. [Online]. Available: https://www.docomo.ne.jp/english/info/media_center/pr/2020/0117_00.html

[27] J. Zhang, Z. Li, L. Shao, and W. Zhu, "Dynamical absorption manipulation in a graphene-based optically transparent and flexible metasurface," *Carbon*, vol. 176, pp. 374–382, May 2021. [Online]. Available: https://www.sciencedirect.com/science/article/pii/S0008622321001573

[28] X. Wang, J. Ding, B. Zheng, S. An, G. Zhai, and H. Zhang, "Simultaneous realization of anomalous reflection and transmission at two frequencies using bi-functional metasurfaces," *Sci. Rep.*, vol. 8, no. 1, p. 1876, Jan. 2018. [Online]. Available: https://doi.org/10.1038/s41598-018-20315-2

[29] C. Huang, A. Zappone, G. C. Alexandropoulos, M. Debbah, and C. Yuen, "Reconfigurable intelligent surfaces for energy efficiency in wireless communication," *IEEE Trans. Wireless Commun.*, vol. 18, no. 8, pp. 4157–4170, Aug. 2019.

[30] E. Björnson, Ö. Özdogan, and E. G. Larsson, "Intelligent reflecting surface vs. decode-and-forward: How large surfaces are needed to beat relaying?" *IEEE Wireless Commun. Lett.*, vol. 9, no. 2, pp. 244–248, Feb. 2020.

[31] K. Ntontin, A.-A. A. Boulogeorgos, D. G. Selimis, F. I. Lazarakis, A. Alexiou, and S. Chatzinotas, "Reconfigurable intelligent surface optimal placement in millimeter-wave networks," *IEEE Open J. Commun. Soc.*, vol. 2, pp. 704–718, Mar. 2021.

[32] S. Abeywickrama, R. Zhang, Q. Wu, and C. Yuen, "Intelligent reflecting surface: Practical phase shift model and beamforming optimization," *IEEE Trans. Commun.*, vol. 68, no. 9, pp. 5849–5863, Sep. 2020.

[33] S. L. Jia, X. Wan, P. Su, Y. J. Zhao, and T. J. Cui, "Broadband metasurface for independent control of reflected amplitude and phase," *AIP Adv.*, vol. 6, no. 4, Apr. 2016, Art. no. 45024.

[34] J. Zhang, X. Wei, I. D. Rukhlenko, H.-T. Chen, and W. Zhu, "Electrically tunable metasurface with independent frequency and amplitude modulations," *ACS Photon.*, vol. 7, no. 1, pp. 265–271, Dec. 2019.

[35] B. Fletcher. "New Samsung 5G phones can tap both sub-6 GHz and millimeter wave spectrum, Samsung." Feb. 2020. [Online]. Available: https://www.fiercewireless.com/devices/new-samsung-5g-phones-can-tap-both-sub-6-ghz-and-millimeter-wave-spectrum

[36] A. Annamalai, G. Deora, and C. Tellambura, "Analysis of generalized selection diversity systems in wireless channels," *IEEE Trans. Veh. Technol.*, vol. 55, no. 6, pp. 1765–1775, Nov. 2006.

[37] E. Björnson and L. Sanguinetti, "Rayleigh fading modeling and channel hardening for reconfigurable intelligent surfaces," *IEEE Wireless Commun. Lett.*, vol. 10, no. 4, pp. 830–834, Apr. 2021.

[38] M. J. Lee, L. Song, S. Yoon, and S. R. Park, "Evaluation of directivity for planar antenna arrays," *IEEE Antennas Propag. Mag.*, vol. 42, no. 3, pp. 64–67, Jun. 2000.
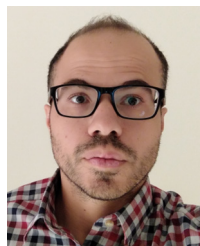
[39] W. Tang et al., "Path loss modeling and measurements for reconfigurable intelligent surfaces in the millimeter-wave frequency band," 2021, *arXiv:1906.09490*.

[40] L. Petrou, K. M. Kossifos, M. A. Antoniades, and J. Georgiou, "The first family of application-specific integrated circuits for programmable and reconfigurable metasurfaces," *Sci. Rep.*, vol. 12, no. 1, p. 5826, Apr. 2022. [Online]. Available: https://doi.org/10.1038/s41598-022-09772-y

[41] A. Annamalai, G. Deora, and C. Tellambura, "Analysis of generalized selection diversity systems in wireless channels," *IEEE Trans. Veh. Technol.*, vol. 55, no. 6, pp. 1765–1775, Nov. 2006.

[42] A. Annamalai and C. Tellambura, "A simple exponential integral representation of the generalized Marcum Q-function QM (a, b) for real-order M with applications," in *Proc. MILCOM IEEE Military Commun. Conf.*, San Diego, CA, USA, 2008, pp. 1–7.

[43] C. Mun, C.-H. Kang, and H.-K. Park, "Approximation of SNR statistics for MRC diversity systems in arbitrarily correlated Nakagami fading channels," *Electron. Lett.*, vol. 35, no. 4, pp. 266–267, Feb. 1999.

Emil Björnson (Fellow, IEEE) received the M.S. degree in engineering mathematics from Lund University, Sweden, in 2007, and the Ph.D. degree in telecommunications from the KTH Royal Institute of Technology (KTH), Sweden, in 2011.

From 2012 to 2014, he was a Postdoctoral Researcher with the Alcatel-Lucent Chair on Flexible Radio, CentraleSupélec, France. From 2014 to 2021, he held different professor positions with Linköping University, Sweden. From 2020 to 2021, he was a part-time Visiting Full Professor with KTH, where he has been a Tenured Full Professor of Wireless Communication since 2022. He has authored the textbooks *Optimal Resource Allocation in Coordinated Multi-Cell Systems* in 2013, *Massive MIMO Networks: Spectral, Energy, and Hardware Efficiency* in 2017, and *Foundations of User-Centric Cell-Free Massive MIMO* in 2021. He is dedicated to reproducible research and has made a large amount of simulation code publicly available. He performs research on MIMO communications, radio resource allocation, machine learning for communications, and energy efficiency. He has performed MIMO research for 16 years, his papers have received more than 18000 citations, and he has filed more than 20 patent applications. He is a host of the podcast Wireless Future and has a popular YouTube channel with the same name.

Dr. Björnson has received the 2014 Outstanding Young Researcher Award from IEEE ComSoc EMEA, the 2015 Ingvar Carlsson Award, the 2016 Best Ph.D. Award from EURASIP, the 2018 and 2022 IEEE Marconi Prize Paper Awards in wireless communications, the 2019 EURASIP Early Career Award, the 2019 IEEE Communications Society Fred W. Ellersick Prize, the 2019 IEEE Signal Processing Magazine Best Column Award, the 2020 Pierre–Simon Laplace Early Career Technical Achievement Award, the 2020 CTTC Early Achievement Award, and the 2021 IEEE ComSoc RCC Early Achievement Award. He also coauthored papers that received Best Paper Awards at the conferences, including WCSP 2009, the IEEE CAMSAP 2011, the IEEE SAM 2014, the IEEE WCNC 2014, the IEEE ICC 2015, and WCSP 2017. He has been on the editorial board of the IEEE TRANSACTIONS ON COMMUNICATIONS since 2017. He has been a member of the online editorial team of the IEEE TRANSACTIONS ON WIRELESS COMMUNICATIONS since 2020. He has been an Area Editor of IEEE Signal Processing Magazine since 2021. He is a Fellow of the Wallenberg Academy and the Digital Futures and an SSF Future Research Leader.

Alexandros-Apostolos A. Boulogeorgos (Senior Member, IEEE) was born in Trikala, Greece, in 1988. He received the Diploma degree in electrical and computer engineering (ECE) and the Ph.D. degree in wireless communications from the Aristotle University of Thessaloniki (AUTh) in 2012 and 2016, respectively.

From 2022, he is an Assistant Professor with the Department of ECE, University of Western Macedonia, Greece. From 2017 to 2022, he served as a Senior Researcher with the Department of Digital Systems, University of Piraeus, where he conducted research in the area of wireless communications. From October 2012 to September 2016, he was a Teaching Assistant with the Department of ECE, AUTh. From February 2017 to September 2022, he served as an Adjunct Professor with the Department of ECE, University of Western Macedonia and as an Visiting Lecturer with the Department of Computer Science and Biomedical Informatics, University of Thessaly. He has worked in a number of EU and national projects. He has coauthored more than 120 technical papers, which were published in scientific journals and presented at prestigious international conferences. Furthermore, he is the holder of two (one national and one European) patents. His current research interests spans in the area of wireless communications and networks with emphasis in high frequency communications, intelligent communication systems, optical wireless communications, and signal processing and communications for biomedical applications.

Dr. Boulogeorgos was awarded the Distinction Scholarship Award from the Research Committee of AUTh in 2014, and was recognized as an Exemplary Reviewer for IEEE COMMUNICATION LETTERS in 2016 (top 3% of reviewers). Moreover, he was named a Top Peer Reviewer (top 1% of reviewers) in Cross-Field and Computer Science in the Global Peer Review Awards in 2019, which was presented by the Web of Science and Publons. Finally, in 2021, he received the Best Oral Presentation Award in the International Conference on Modern Circuits and Systems Technologies. He has been involved as a member of organizational and technical program committees in several IEEE and non-IEEE conferences and served as a reviewer in various IEEE journals and conferences. He is currently an Editor for IEEE COMMUNICATIONS LETTERS, an Associate Editor for the *Frontier in Communications and Networks*, and for the *Telecom* (MDPI). Finally, he has participated as a guest editor in the organization of a number of special issues in IEEE and non-IEEE journals. He is a Member of the Technical Chamber of Greece.

Konstantinos Ntontin (Member, IEEE) received the Diploma degree in electrical and computer engineering from the University of Patras, Greece, in 2006, the M.Sc. degree in wireless systems from the Royal Institute of Technology (KTH), Sweden, in 2009, and the Ph.D. degree from the Technical University of Catalonia, Spain, in 2015. He is currently a Research Scientist with the SIGCOM Research Group at SnT, University of Luxembourg. In the past, he held research associate positions with the Electronic Engineering and Telecommunications Department, University of Barcelona, the Informatics and Telecommunications Department, University of Athens, and the National Centre of Scientific Research-"Demokritos." In addition, he held an internship position with Ericsson Eurolab Gmbh, Germany. His research interests are related to the physical layer of wireless telecommunications with focus on performance analysis in fading channels, MIMO systems, array beamforming, transceiver design, and stochastic modeling of wireless channels.

Zaid Abdullah (Member, IEEE) received the Ph.D. degree in communications and signal processing from Newcastle University, U.K., in 2019. He is currently a Research Associate with SnT, University of Luxembourg. He was a Postdoctoral Research Assistant with the School of Engineering, University of Leicester, U.K., from 2019 to 2021. He is passionate about the research on large-scale antenna arrays, space–air–ground integrated networks, and artificial intelligence.

Sergi Abadal (Member, IEEE) received the B.Sc. and M.Sc. degrees in telecommunication engineering from the Universitat Politècnica de Catalunya (UPC), Barcelona, Spain, in 2010 and 2011, respectively, and the Ph.D. degree in computer architecture from the Department of Computer Architecture, UPC, in July 2016. He held several visiting researcher positions at the Georgia Institute of Technology, the University of Illinois at Urbana–Champaign, and the Foundation for Research and Technology, Greece. He is currently working as a Distinguished Researcher with the NaNoNetworking Center in Catalonia Group, Department of Computer Architecture, UPC. His current research interests include chip-scale wireless communications, including channel modeling and protocol design, and the application of these techniques for the creation of novel architectures for next-generation classical and quantum computing systems. He was a recipient of the Starting Grant, called WINC, from the European Research Council and a Project Coordinator of WIPLASH H2020 FET-OPEN Project. He has participated in several other national and EU projects. He is an Area Editor of the *Nano Communication Networks Journal* (Elsevier), where he was selected as an Editor in 2019. Since 2020, he has been acting as one of the Ambassadors of the European Innovation Council through its program of National Champions. He is a member of ACM and HiPEAC.

Agapi Mesodiakaki (Member, IEEE) received the five-year Diploma (M.Sc.) degree in electrical and computer engineering from the National Technical University of Athens in 2011, and the Ph.D. degree (cum laude) from the Signal Theory and Communications Department (TSC), Universitat Politécnica de Catalunya, Barcelona, in November 2015. She was granted the prestigious Marie-Curie Early-Stage-Researcher scholarship in 2011. Her Ph.D. dissertation was awarded as one of the best dissertations of the year receiving a Special Doctoral Award (PREMIO EXTRAORDINARIO DE DOCTORADO). During her Ph.D. studies, she completed two secondments with Cassidian (Airbus Defense and Space Group) in France, and WEST Aquila S.r.l., Italy. The following years after the Ph.D., she worked as a Postdoctoral Researcher with Karlstad University, Sweden. Since January 2018, she has been a Senior Researcher with the Department of Informatics, Aristotle University of Thessaloniki, and a Member of the Wireless and Photonic Systems and Networks (WinPhoS) Research Group of the Center for Interdisciplinary Research and Innovation. She has authored more than 50 research papers in peer-reviewed journals and international conferences. Her main research interests include energy-efficient radio resource management techniques for wireless communication networks, cognitive radio networks, mmWave, B5G and 6G, converged fiber-wireless networks, energy harvesting, and optimization theory.

Symeon Chatzinotas (Fellow, IEEE) received the M.Eng. degree in telecommunications from the Aristotle University of Thessaloniki, Thessaloniki, Greece, in 2003, and the M.Sc. and Ph.D. degrees in electronic engineering from the University of Surrey, Surrey, U.K., in 2006 and 2009, respectively. He is currently a Full Professor/Chief Scientist I and the Head of the SIGCOM Research Group at SnT, University of Luxembourg. In the past, he was a Visiting Professor with the University of Parma, Italy, and he was involved in numerous research and development projects for the National Center for Scientific Research Demokritos, the Center of Research and Technology Hellas, and the Center of Communication Systems Research, University of Surrey. He has (co)authored more than 500 technical articles in refereed international journals, conferences, and scientific books. He was a co-recipient of the 2014 IEEE Distinguished Contributions to Satellite Communications Award, the CROWNCOM 2015, 2018 EURASIC JWCN, and 2022 WCNC Paper Award. He is currently on the editorial board of the IEEE TRANSACTIONS ON COMMUNICATIONS, IEEE OPEN JOURNAL OF VEHICULAR TECHNOLOGY, and the *International Journal of Satellite Communications and Networking*.